

Published in final edited form as:

Mon Not R Astron Soc. 2018 July ; 477(3): 3694–3710. doi:10.1093/mnras/sty834.

Maximally rotating supermassive stars at the onset of collapse: the perturbative effects of gas pressure, magnetic fields, dark matter, and dark energy

Satya P. Butler¹, Alicia R. Lima¹, Thomas W. Baumgarte^{1,*}, and Stuart L. Shapiro^{2,3}

¹Department of Physics and Astronomy, Bowdoin College, Brunswick, ME 04011, USA

²Department of Physics, University of Illinois at Urbana-Champaign, Urbana, IL 61801, USA

³Department of Astronomy and NCSA, University of Illinois at Urbana-Champaign, Urbana, IL 61801, USA

Abstract

The discovery of quasars at increasingly large cosmological redshifts may favour ‘direct collapse’ as the most promising evolutionary route to the formation of supermassive black holes. In this scenario, supermassive black holes form when their progenitors – supermassive stars – become unstable to gravitational collapse. For uniformly rotating stars supported by pure radiation pressure and spinning at the mass-shedding limit, the critical configuration at the onset of collapse is characterized by universal values of the dimensionless spin and radius parameters J/M^2 and R/M , independent of mass M . We consider perturbative effects of gas pressure, magnetic fields, dark matter, and dark energy on these parameters, and thereby determine the domain of validity of this universality. We obtain leading-order corrections for the critical parameters and establish their scaling with the relevant physical parameters. We compare two different approaches to approximate the effects of gas pressure, which plays the most important role, find identical results for the above dimensionless parameters, and also find good agreement with recent numerical results.

Keywords

black hole physics; equation of state; stars: Population III

1 INTRODUCTION

Quasars and active galactic nuclei, believed to be powered by accreting supermassive black holes (SMBHs), are observed out to large cosmological distances (see e.g. Fan 2006; Fan et al. 2006). Bañados et al. (2018) recently announced the discovery of the most distant quasar ever observed, J1342+0928, at a redshift of $z \approx 7.5$, and powered by an SMBH with mass of approximately $7.8 \times 10^8 M_{\odot}$. The previous distance-record holder was J1120–0641, at a

* tbaumgar@bowdoin.edu.

This paper has been typeset from a TeX/LaTeX file prepared by the author.

redshift of $z \approx 7.1$ and with a black hole mass of approximately $2.0 \times 10^9 M_{\odot}$ (Mortlock et al. 2011). Another remarkable object is the ultraluminous quasar J0100+2802 discovered by Wu et al. (2015), at a redshift of $z = 6.3$ and with a mass of about $1.2 \times 10^{10} M_{\odot}$. The detection of these objects poses an important astrophysical problem that has attracted significant attention (see e.g. Shapiro 2004; Haiman 2013; Latif & Ferrara 2016; Smith, Bromm & Loeb 2017, for reviews): how could such massive black holes form in such a short time after the big bang?

One evolutionary scenario for the formation of SMBH invokes first generation – i.e. Population III (Pop III) – stars (Madau & Rees 2001; Heger & Woosley 2002). These stars could collapse to form seed black holes (Fryer, Woosley & Heger 2001; Heger et al. 2003) at large cosmological redshift, which, conceivably, could then grow through accretion and/or mergers to form SMBHs. For a given efficiency ϵ of the conversion of matter to radiation, growth by accretion is usually limited by the Eddington luminosity (Shapiro 2005; Pacucci, Volonteri & Ferrara 2015). It has been suggested that episodic super-Eddington accretion may speed up the growth of seed black holes (Volonteri & Rees 2005; Volonteri, Silk & Dubus 2015; Lupi et al. 2016; Sakurai, Inayoshi & Haiman 2016). On the other hand, the effects of photoionization and heating appear to reduce accretion to only a fraction of the Eddington limit [see Alvarez, Wise & Abel 2009; Milosavljević et al. 2009, see also Whalen & Fryer (2012) for the effect of natal kicks on the accretion rate]. Black holes can also grow through mergers (see e.g. Volonteri, Haardt & Madau 2003a; Volonteri, Madau & Haardt 2003b; Shapiro 2005; Tanaka & Haiman 2009; Tanaka 2014), even though some limits on growth by mergers may be imposed by recoil speeds (Haiman 2004).

Given these constraints, it is difficult to see how seed black holes with masses of Pop III stars, about $100 M_{\odot}$, could grow to the masses of SMBHs by $z \approx 7$. In fact, Bañados et al. (2018) argue that the existence of the objects J1342+0928, J1120–0641, and J0100+2802 ‘is at odds with early black hole formation models that do not involve either massive ($\gtrsim 10^4 M_{\odot}$) seeds or episodes of hyper-Eddington accretion’ (see also their fig. 2). These considerations suggest the direct collapse of objects with masses of $M \gtrsim 10^4 - 5 M_{\odot}$ as a plausible alternative scenario for the formation of SMBHs (e.g. Rees 1984; Loeb & Rasio 1994; Oh & Haiman 2002; Bromm & Loeb 2003; Koushiappas, Bullock & Dekel 2004; Shapiro 2004; Lodato & Natarajan 2006; Begelman, Volonteri & Rees 2006; Regan & Haehnelt 2009b; Begelman 2010; Agarwal et al. 2012; Johnson et al. 2013).

The ‘direct-collapse’ scenario assumes that the progenitor object, which we will refer to as a supermassive star (SMS), is able to avoid fragmentation. Physical processes that help suppress fragmentation are turbulence (e.g. Wise, Turk & Abel 2008; Latif et al. 2013; Mayer et al. 2015) and a Lyman–Werner radiation background (see Bromm & Loeb 2003; Regan & Haehnelt 2009a; Visbal, Haiman & Bryan 2014, and references therein). The Lyman–Werner radiation dissociates molecular hydrogen, the most efficient coolant in metal-free haloes, which otherwise would allow the halo to cool to such low temperatures that its Jeans mass would become small compared to its mass itself, thereby leading to fragmentation (see also Li, Klessen & Mac Low 2003). In fact, the recent discovery of the strong Lyman- α emitter CR7 at $z = 6.6$ (Sobral et al. 2015) has been interpreted as observational evidence of the direct collapse scenario [see Smith, Bromm & Loeb 2016;

Hartwig et al. 2016; Agarwal et al. 2016; also see Bowler et al. (2017); Agarwal et al. (2017) for a discussion of the role of metals in this object].

The formation, evolution, stability, and collapse of SMSs have been the subject of numerous studies over several decades (see e.g. Iben 1963; Hoyle & Fowler 1963; Chandrasekhar 1964; Bisnovaty-Kogan, Zel'dovich & Novikov 1967; Wagoner 1969; Appenzeller & Fricke 1972; Begelman & Rees 1978; Fuller, Woosley & Weaver 1986 for some early references, as well as Zeldovich & Novikov 1971 and Shapiro & Teukolsky 1983, hereafter ST, for textbook treatments). While the existence of SMSs had been considered somewhat hypothetical for many years, and while many questions concerning the formation of SMSs remain open (see e.g. Schleicher et al. 2013; Hosokawa et al. 2013; Sakurai et al. 2015; Umeda et al. 2016; Woods et al. 2017; Haemmerlé et al. 2018b, 2018a for recent studies; see also Smith et al. 2017), the discovery of objects like J1342+0928, J1120–0641, and J0100+2802 and CR7 suggests that they not only exist, but that they played a key role in the formation of SMBHs.

These considerations have motivated us to revisit an idealized evolutionary scenario for rotating SMSs that two of us proposed previously (see Baumgarte & Shapiro 1999b, hereafter Paper I). Specifically, we assumed that SMSs are dominated by radiation pressure, and that turbulent viscosity produced by magnetic fields transports angular momentum sufficiently efficiently to maintain uniform rotation (Bisnovaty-Kogan et al. 1967; Wagoner 1969). We further assumed that SMSs, after initially formed, cool and contract, leading to a spin-up. Given our assumption of uniform rotation, the star will ultimately reach mass shedding, i.e. the *Kepler* limit. While it has been suggested that SMSs formed from accretion only rotate at a fraction of the mass-shedding limit (e.g. Maeder & Meynet 2000; Haemmerlé et al. 2018b), such stars may still reach mass shedding during subsequent cooling and contraction. It is also possible that alternative formation scenarios lead to SMSs that rotate rapidly, arriving at mass shedding either initially or during subsequent cooling and contraction. Once having reached the *Kepler* limit, the SMS evolves along the mass-shedding limit (at a rate computed in Baumgarte & Shapiro 1999a) until it reaches an onset of radial instability, triggering collapse to a black hole. The onset of instability is a consequence of the interplay between the stabilizing effects of rotation and the destabilizing effects of relativistic gravitation. Remarkably, the critical configuration marking the onset of instability is characterized by unique values of the dimensionless parameters J/M^2 and R_p/M , where J is the total angular momentum, M the mass, and R_p the polar radius. The equatorial radius is given by $R_{\text{eq}} = 3R_p/2$.

The uniqueness of these parameters has profound implications for the subsequent collapse to black holes, because it then has to follow a unique evolutionary track as well. A number of authors have studied this rotating collapse numerically in the context of general relativity, starting with Shibata & Shapiro (2002) (see also Shapiro & Shibata 2002 for a related analytical treatment). The collapse results in a spinning black hole with mass $M_{\text{BH}}/M \approx 0.9$ and angular momentum $J_{\text{BH}}/M_{\text{BH}} \approx 0.7$, surrounded by a disc with mass $M_{\text{disc}}/M \approx 0.1$. The universal evolutionary track also emits a universal gravitational wave signal (Shibata et al. 2016a; Sun et al. 2017), which might serve as a ‘standard candle’ for future space-based

gravitational wave detectors. Observations of this ‘signature’ gravitational wave signal would firmly establish SMSs as the progenitors of SMBHs.

The original simulations of Shibata & Shapiro (2002), who modelled the star as an ideal radiation fluid, were followed up by several other studies in general relativity that also allowed for gas pressure (Shibata et al. 2016a), nuclear reactions (Montero, Janka & Müller 2012; Uchida et al. 2017), as well as magnetic fields (Liu, Shapiro & Stephens 2007; Sun et al. 2017). The latter demonstrate that this collapse may result in the launch of a jet and power ultralong gamma-ray bursts, and suggest that collapsing SMSs are promising multimessenger sources for coincident gravitational and electromagnetic radiations.

Given the importance of the dimensionless parameters describing the critical configurations, it is of interest to evaluate to what degree their universality depends on the assumptions made in their derivation – in particular the assumption of a pure radiation fluid – and to establish the domain of validity of this universality. In this paper, we develop an analytic perturbational approach to study the effects of gas pressure, magnetic fields, dark matter (DM), and dark energy on the critical configuration of maximally rotating SMSs and its dimensionless parameters; our results are summarized in equations (142) and (143) below. For the astrophysical scenarios that we consider most realistic, gas pressure plays the most important perturbative role by far. Accordingly, most of our paper focuses on gas pressure. We compare two different approximations that have been adopted to account for gas pressure (see Sections 2.4 and 2.5 below), and calibrate these two different approaches for non-rotating stars (Section 3) before applying them to maximally rotating SMSs (Section 5).

Our perturbative approach builds on an analytical calculation employing a simple energy functional and variational principle that we adopted in Paper I to identify the critical configuration (see Sections 4.1 and 4.2 below). In a completely independent approach, we also constructed numerically fully relativistic equilibrium models of rotating stars in Paper I. We found good agreement in the parameters characterizing the critical configuration between the two approaches (see table 2 in Paper I as well as Table 2 below); typically these parameters agree to within 10 per cent or better. Shibata, Uchida & Sekiguchi (2016b, hereafter SUS) recently generalized these numerical results, adopting what we refer to below as Approach II to approximate the effects of gas pressure. Our analytic calculation presented here complements those numerical results: we find good agreement between our analytical results and the numerical results of SUS (see e.g. Fig. 3 below), and we also extend our analytical treatment to account for the effects of magnetic fields, DM, and dark energy (Section 6).

This paper is organized as follows. In Section 2, we review some thermodynamic relations. In particular, we discuss in Sections 2.4 and 2.5, the two different approaches to modelling gas pressure as a small perturbation to radiation pressure. In Section 3, we compare these two approaches for non-rotating SMSs. We construct numerical models in Section 3.1, and use these to calibrate an analytical model calculation in Section 3.2. In Section 4, we extend the analytical model calculations to rotating SMSs. We review the general set-up from Paper I and compute the unperturbed background solution in Sections 4.1 and 4.2, and develop a general framework for perturbations in Section 4.3. In Section 5, we return to the effects of

gas pressure. We adopt Approaches I and II in Sections 5.1 and 5.2, compare with the numerical results of SUS in Section 5.3, and provide estimates for physical parameters in Section 5.4. In Section 6, we apply our perturbative approach to estimate the effects of magnetic fields, a DM halo, and dark energy on the critical configuration of SMSs that are uniformly rotating at the mass-shedding limit. We provide a brief summary in Section 7.

Unless noted otherwise, we adopt geometrized units with $c = G = 1$.

2 THERMODYNAMIC PRELIMINARIES

In this section, we review some thermodynamic relations, following the treatment in several textbooks (e.g. ST as well as Clayton 1983; Kippenhahn, Weigert & Weiss 2012). While most of these relations are well known, we list them here for an easier comparison of two different approaches to modelling the effect of gas pressure on SMSs, which we introduce in Sections 2.4 and 2.5.

2.1 Radiation pressure

For a pure thermal radiation fluid the pressure P_r is given by

$$P_r = \frac{1}{3}aT^4, \quad (1)$$

and the internal energy density ϵ_r by

$$\epsilon_r = aT^4, \quad (2)$$

where T is the temperature and a the radiation constant

$$a = \frac{8\pi^5 k_B^4}{15c^3 h^3} \quad (3)$$

(with $c=1$ in geometrized units). Here, k_B is the Boltzmann constant and h is *Planck's* constant. From the first law of thermodynamics

$$T ds = d\left(\frac{\epsilon}{n_B}\right) + P d\left(\frac{1}{n_B}\right), \quad (4)$$

where n_B is the baryon number density, we find that the photon entropy per baryon is

$$s_r = \frac{4a T^3}{3 n_B}. \quad (5)$$

Combining equations (1) and (5), we can write the pressure as

$$P_r = K_r \rho_0^\Gamma \quad (6)$$

with $\Gamma = 1 + 1/n = 4/3$. Here, $\rho_0 = n_B m_B$ is the rest-mass density, with m_B the baryon rest mass, and we have defined

$$K_r \equiv \frac{a}{3} \left(\frac{3s_r}{4m_B a} \right)^{4/3}. \quad (7)$$

Evidently, stars dominated by radiation pressure behave as $n = 3$ polytropes for constant entropy.

2.2 Gas pressure

If gas pressure cannot be neglected, the total pressure and internal energy density are given by

$$P = P_r + P_g \quad (8)$$

and

$$\varepsilon = \varepsilon_r + \varepsilon_g, \quad (9)$$

where

$$P_g = Y_T n_B k_B T \quad (10)$$

is the gas pressure and

$$\epsilon_g = \frac{3}{2} Y_T n_B k_B T \quad (11)$$

the internal energy density of the plasma. Here, Y_T is the number of particles per baryon. For simplicity, we will assume a fully ionized hydrogen gas in the following, in which case $Y_T = 2$. The total entropy per baryon is then given by

$$s = s_r + s_g, \quad (12)$$

where s_g is the gas entropy

$$\frac{s_g}{k_B} = \ln \left(4 \frac{m_e^{3/2} m_B^{3/2}}{n_B^2} \left(\frac{k_B T}{2\pi\hbar^2} \right)^3 \right) + 5 = \ln \frac{T^3}{\rho_0^2} + \frac{s_0}{k_B} \quad (13)$$

with

$$\frac{s_0}{k_B} = 3 \ln \left(\frac{k_B}{2\pi\hbar^2} \right) + \frac{3}{2} \ln m_e + \frac{7}{2} \ln m_B + 2 \ln 2 + 5 \quad (14)$$

[see equation (17.3.4) in ST; hereafter equation (ST.17.3.4)]. Here, m_e is the electron mass.

2.3 Eddington's argument

The Eddington standard model (Eddington 1918a; see also Chandrasekhar 1939; Clayton 1983; Kippenhahn et al. 2012, as well as many other references) is based on the observation that, if the ratio¹

$$\beta \equiv \frac{P_g}{P_r} = \frac{8k_B}{s_r} \quad (15)$$

is constant throughout a given star, then the star again behaves like an $n = 3$ polytrope, i.e. the total pressure again satisfies a polytropic relation

$$P = K_E \rho_0^\Gamma \quad (16)$$

¹In many texts, the ratio β is alternatively defined to refer to the ratio P_g/P_r rather than P_g/P_r .

with $\Gamma = 4/3$. This can be seen by writing

$$P = (1 + \beta)P_r = \frac{1 + \beta}{3}aT^4. \quad (17)$$

This relation can now be used to eliminate T in terms of P in both terms on the right-hand side of (8). Solving the result for P yields equation (16) with

$$K_E = (1 + \beta)\frac{a}{3}\left(\frac{3s_r}{4m_B a}\right)^{4/3} = (1 + \beta)K_r. \quad (18)$$

As expected, K_E reduces to K_r in the limit $\beta \rightarrow 0$.

Under certain circumstances, it is reasonable to approximate β as constant. SMSs are expected to be convective, however (see e.g. Loeb & Rasio 1994), which makes it more realistic to assume the *total* entropy s , rather than the radiation entropy s_r in equation (15), to be constant inside a given star. This assumption forms the basis of our first approach to modelling the effects of gas pressure on SMSs.

2.4 Effects of gas pressure: Approach I

In what we call ‘Approach I’, we follow Section 17.3 in ST to treat the gas pressure as a small perturbation to the radiation pressure at constant total entropy s . Specifically, we assume that $s_g \ll s_r$ in equation (12), so that, to zeroth order, the temperature is given by equation (5) with s_r replaced by s . The leading-order correction to the temperature in terms of s can then be computed by inserting equations (5) and (13) into equation (12); this results in

$$T \simeq \left(\frac{3s\rho_0}{4m_B a}\right)^{1/3} \left(1 - \frac{s_0}{3s} - \frac{k_B}{3s} \ln \frac{3s}{4m_B a \rho_0}\right) \quad (19)$$

[see equation (ST.17.3.9)]. Inserting this into equation (9) then yields

$$\epsilon \simeq K_1 \rho_0^{4/3} (3 + \bar{\lambda} + \bar{\mu} \ln \rho_0). \quad (20)$$

Here, we defined

$$K_I \equiv \frac{a}{3} \left(\frac{3s}{4m_B a} \right)^{4/3}, \quad (21)$$

and the coefficients $\bar{\lambda}$ and $\bar{\mu}$ are given by

$$\bar{\lambda} = -\frac{4s_0}{s} + \frac{12k_B}{s} - \frac{4k_B}{s} \ln \frac{3s}{4m_B a} \quad (22)$$

and

$$\bar{\mu} = \frac{4k_B}{s}. \quad (23)$$

ST list the related coefficients $\lambda = K_I \bar{\lambda}$ and $\mu = K_I \bar{\mu}$ in their equations (ST.17.3.11) and (ST.17.3.12).

Since $\bar{\lambda}$ and $\bar{\mu}$ describe leading-order corrections, we may replace s in equations (22) and (23) with s_r , which, using equation (15), can then be expressed in terms of β . Also inserting equations (14) and (3) into equations (22) and (23), we obtain

$$\varepsilon \simeq K_I \rho_0^{4/3} \left(3 - \beta \left(1 - \frac{5}{2} \ln \beta - \frac{1}{2} \ln (K_I^3 \rho_0) + \frac{1}{2} \ln \eta \right) \right), \quad (24)$$

where we have used the abbreviation

$$\eta = \frac{2^4 3^4 5^2}{\pi^7} \left(\frac{m_e}{m_B} \right)^{3/2} \simeq 1.367 \times 10^{-4}. \quad (25)$$

We note that, in geometrized units, the combination $K_I^3 \rho_0$ is dimensionless (see Section 3.1 below), so that all arguments of logarithms in equation (24) are dimensionless numbers.

For a given value of the entropy s , the internal energy density ε is given as a function of the rest-mass density ρ_0 by (24). The pressure P can be computed by observing that

$$\varepsilon = 3P_r + \frac{3}{2}P_g = 3 \left(1 + \frac{\beta}{2} \right) P_r \quad (26)$$

and therefore

$$P = (1 + \beta) P_r = \frac{1}{3} \frac{1 + \beta}{1 + \beta/2} \epsilon. \quad (27)$$

Since P_g is again considered a small correction to P_r , we can again approximate β as given by equation (15) with s_r replaced by s in these leading-order correction terms. For $\beta \rightarrow 0$, we evidently recover the radiation-fluid expressions of Section 2.1. We note that, for non-zero β , Approach I does not assume the equation of state (EOS) to be of polytropic form.

2.5 Effects of gas pressure: Approach II

An alternative approach to approximating the effects of gas pressure is based on the observation that, in the presence of both radiation and gas pressure, the adiabatic exponent is given by

$$\Gamma_1 \equiv \left(\frac{d \ln P}{d \ln \rho_0} \right)_s = \frac{4}{3} + \frac{\beta(4 + \beta)}{3(1 + \beta)(8 + \beta)} \simeq \frac{4}{3} + \frac{\beta}{6}, \quad (28)$$

where β is again given by equation (15) (see e.g. Eddington 1918b; Chandrasekhar 1939; Bond, Arnett & Carr 1984; see also Problem 17.3 in ST and Problem 2.26 in Clayton 1983). This suggests that we may approximate the EOS as

$$P = K_{\text{II}} \rho_0^{\Gamma_1}. \quad (29)$$

Using the arguments of Section 2.3, we find

$$K_{\text{II}} = K_{\text{E}} \rho_0^{-\beta/6} \quad (30)$$

with K_{E} given by equation (18) [compare, for example equation (7) in SUS]. Evidently, K_{II} is only approximately constant for small, but non-zero β . Approximating K_{II} as constant, however, the internal energy density is given by

$$\epsilon = n_1 P \quad (31)$$

where

$$n_1 = \frac{1}{\Gamma_1 - 1} = \frac{3}{1 + \beta/2} \quad (32)$$

is the approximate polytropic index.

3 EFFECTS OF GAS PRESSURE ON NON-ROTATING SMSS

In this section, we adopt both Approaches I and II to consider the effects of gas pressure on non-rotating stars. While most of these results can be found in the literature, nowhere are the two approaches carefully distinguished or compared. Hence, we include this section in order to (i) compare predictions from Approaches I and II, and (ii) calibrate an analytical model that we will apply to rotating stars in Section 5.

3.1 Numerical results

The structure of a relativistic, spherically symmetric SMS is governed by the Tolman–Oppenheimer–Volkoff (TOV) equations

$$\begin{aligned} \frac{dm}{dr} &= 4\pi(\rho_0 + \varepsilon)r^2 \\ \frac{dP}{dr} &= -(\rho_0 + \varepsilon + P)\frac{m + 4\pi Pr^3}{r^2(1 - 2m/r)}, \end{aligned} \quad (33)$$

where $m(r)$ is the mass enclosed within a radius r , and $M = m(R)$ is the total mass, with R being the stellar radius (see Oppenheimer & Volkoff 1939; Tolman 1939).

In geometrized units, ε and ρ_0 have the same units of inverse length squared. From equations (26) and (31), we therefore see that $K^{n/2}$ must have units of length, where $K=K_I$ and $n=3$ in Approach I, and $K=K_{II}$ and $n=n_1$ in Approach II (note, though, that the EOS is not assumed to be of polytropic form in Approach I). In either approach, we may therefore introduce dimensionless quantities, for example $m\bar{=} K^{-n/2}m$ and $\bar{\rho}_0 = K^n\rho_0$. When written in terms of these dimensionless quantities, the TOV equations (33), together with equations (26) and (27) in Approach I and equations (29) and (31) in Approach II, become independent of the constants K .

We construct sequences of TOV solutions and find, for given values of β , the stellar mass \bar{M} as a function of central rest-mass density $\bar{\rho}_c$. From these, we also compute the dimensionless variable

$$x \equiv \bar{M}^{2/3}\bar{\rho}_c^{-1/3} = M^{2/3}\rho_c^{1/3}. \quad (34)$$

The maximum-mass configuration marks a turning point in the curve of \bar{M} versus x , at which stars become unstable to radial collapse. We record the corresponding critical values \bar{M}_{crit} and x_{crit} . For $\beta = 0$, the maximum mass is found for zero density (i.e. the curve is monotonically decreasing with x and there is no turning point) and takes the well-known Newtonian value

$$\bar{M}_0^{\text{sph}} = 4.555 \quad (35)$$

which we rederive below in equation (39). Such a non-rotating SMS without gas pressure is thus unstable at all finite radii. For small but non-zero β , we may then write

$$\bar{M}_{\text{crit}} = \bar{M}_0^{\text{sph}} (1 + \delta_M^{\text{sph}}). \quad (36)$$

In Figs 1 and 2, we show results for both x_{crit} and δ_M^{sph} as found from Approaches I and II, which show that gas pressure can stabilize an SMS below a critical central density. We will postpone a more detailed discussion until Section 3.3 below.

3.2 Analytical model

The mass and density of non-rotating SMSs can be estimated analytically from an energy variational principle (see Zeldovich & Novikov 1971, and ST).

3.2.1 General set-up—We start by writing the energy as the sum of the internal energy, the gravitational potential energy, and a first post-Newtonian correction to the potential energy,

$$E = k_1 K M \rho_c^{1/n} - k_2 M^{5/3} \rho_c^{1/3} - k_4 M^{7/3} \rho_c^{2/3} \quad (37)$$

(see e.g. Lai, Rasio & Shapiro 1993; Baumgarte & Shapiro 1999b). Here, the polytropic structure constants k_i can be found from the corresponding integrals of Lane–Emden functions. We list numerical values for $n = 3$, which describes SMSs to leading order, in Table 1. It is again convenient to write the above expression in terms of dimensionless quantities. With $\bar{M} = K^{-n/2} M$ and $\bar{E} = K^{-n/2} E$ as well as the dimensionless variable x defined in equation (34), we obtain

$$\bar{E} = k_1 \bar{M}^{1-2/n} x^{3/n} - k_2 \bar{M} x - k_4 \bar{M} x^2. \quad (38)$$

Equilibrium configurations can be found by setting to zero the first derivative of equation (38) with respect to x , at constant mass \bar{M} . For a pure radiation fluid with $n = 3$, this yields the equilibrium mass

$$\bar{M}_0^{\text{sph}} = \left(\frac{k_1}{k_2}\right)^{3/2} = 4.555 \quad (39)$$

for $x = 0$ [cf. equation (35)]. This is the unique value of the mass in Newtonian gravitation, where the last term in equation (38) disappears. Using $M = K^{3/2}\bar{M}$ and inserting equations (7), (15), as well as (39) for \bar{M} , we see that, to leading order, the mass M is related to β by

$$\beta \simeq 8.46 \left(\frac{M}{M_\odot}\right)^{-1/2}. \quad (40)$$

The critical configuration can then be found by also setting to zero the second derivative with respect to x . For a pure radiation fluid this is not possible, correctly reproducing the well-known result that all $n = 3$ polytropes, in particular all stars governed by pure radiation pressure, are unstable in general relativity. They can be stabilized by, e.g. gas pressure (e.g. ST) and/or rotation (Paper I). We now account for the presence of gas pressure using both Approaches I and II.

3.2.2 Approach I—From equation (26) we see that, in Approach I, the internal energy behaves like that of an $n = 3$ polytrope plus a correction. The total internal energy, computed from the integral

$$E_{\text{int}} = 4\pi \int \varepsilon r^2 dr, \quad (41)$$

therefore results in the unperturbed term $E_{\text{int},0} = k_1 K_I M \rho_c^{1/3}$ plus a correction E_{int} . Using equation (26), and following the treatment in Section 17.3 of ST, this correction can be written as

$$\Delta \bar{E}_{\text{int}} = k_1 \bar{M}^{1/3} x \beta \left(\frac{1}{2} \ln x + \frac{5}{6} \ln \beta + C \right). \quad (42)$$

Here, we used the same dimensional rescaling as above, i.e. $\Delta \bar{E} = K_I^{-n/2} \Delta E$ with $n = 3$, we have abbreviated

$$C = \frac{k_r}{2} - \frac{1}{3} \ln \bar{M} - \frac{1}{6} \ln \eta - \frac{1}{3} \quad (43)$$

where $\eta \simeq 1.367 \times 10^{-4}$ is again given by equation (25), and we have defined²

$$k_\tau \equiv \frac{3}{k_1 |\theta'_n| \xi_n^2} \int \theta^{n+1} \ln \theta \xi^2 d\xi = -0.45928. \quad (44)$$

Here, θ is the Lane–Emden density function, defined so that $\rho = \rho_c \theta^n$, ξ is the Lane–Emden radial function, and the last equality holds for $n = 3$ polytropes. Following the treatment in Section 17.3 in ST, we assume that the mass distribution remains that of an $n = 3$ polytrope; in particular, this means that we will adopt the structure coefficients k_i as listed in Table 1.

Adding equations (42) to (38) and setting $n = 3$, we obtain

$$\bar{E} = k_1 \bar{M}^{1/3} x \left(1 + \beta \left(\frac{1}{2} \ln x + \frac{5}{6} \ln \beta + C \right) \right) - k_2 \bar{M} x - k_1 \bar{M} x^2. \quad (45)$$

We now set the first two derivatives of equation (45) to zero and divide by \bar{M} , which results in the equations

$$0 = k_1 \bar{M}^{-2/3} \left(1 + \beta \left(\frac{1}{2} \ln x + \frac{5}{6} \ln \beta + C \right) \right) + \frac{\beta}{2} k_1 \bar{M}^{-2/3} - k_2 - 2k_4 x \quad (46)$$

and

$$0 = \frac{\beta}{2} k_1 \bar{M}^{-2/3} x^{-1} - 2k_4. \quad (47)$$

From equation (47), we obtain

$$x_{\text{crit}} = \frac{k_1}{4k_4} \bar{M}^{-2/3} \beta. \quad (48)$$

²With this definition, the term τ defined in equation (ST.17.3.15) becomes $\tau = k_\tau K_1 \beta / 2$.

Inserting $\beta = 0$ and $x = 0$ into equation (46), we recover the result (39), $\bar{M}_0^{\text{sph}} = (k_1/k_2)^{3/2}$, which we can now insert into equation (48) to find

$$x_{\text{crit}} = \frac{k_2}{4k_4}\beta. \quad (49)$$

Equation (49) shows that for stars of nearly the same mass, a higher ratio of gas to radiation pressure allows a higher central density, or larger compaction, before the star becomes radially unstable to collapse. This is the stabilizing role of gas pressure. As we will see in Section 3.2.3 below, we will find the same result in Approach II; it is included as the solid line in Fig. 1. We note already the excellent agreement with the numerical results of Section 3.1 for small β .

In order to obtain an expression for the correction to the mass at the critical point, we insert equations (47) and (49) and

$$\bar{M} = \bar{M}_0^{\text{sph}}(1 + \delta_M^{\text{sph}}) \quad (50)$$

into equation (46) and expand to leading order to obtain

$$\delta_M^{\text{sph, I}} = \left(\frac{3}{4} \ln \frac{k_2}{4k_4} + 2 \ln \beta + \frac{3}{2} C \right) \beta, \quad (51)$$

where the superscript ‘I’ refers to Approach I. Since δ_M^{sph} already describes a leading-order correction, we may replace \bar{M} with \bar{M}_0^{sph} in C . The prediction (51) is included in Fig. 2 as a solid line. Note that, for small β , this expression is dominated by the term proportional to $\beta \ln \beta$.

3.2.3 Approach II—In Approach II, we simply adopt $n = n_1$, as given in equation (32), in the energy functional equation (38), which then becomes

$$\bar{E} = k_1 \bar{M}^{1/3 - \beta/3} x^{1 + \beta/2} - k_2 \bar{M} x - k_4 \bar{M} x^2. \quad (52)$$

We now use the dimensional rescaling introduced above with K_{II} and n_1 , e.g. $\bar{E} = K_{\text{II}}^{-n_1/3} E$, where we approximate K_{II} as a constant [see equation (30)]. Setting the first two derivatives of equation (52) to zero and dividing by \bar{M} now yields

$$0 = \left(1 + \frac{\beta}{2}\right) k_1 \bar{M}^{-2/3 - \beta/3} x^{\beta/2} - k_2 - 2k_4 x \quad (53)$$

and

$$0 = \frac{\beta}{2} \left(1 + \frac{\beta}{2}\right) k_1 \bar{M}^{-2/3 - \beta/3} x^{\beta/2 - 1} - 2k_4. \quad (54)$$

As in Approach I, we will ignore changes in the structure constants k_i .

Combining equations (53) and (54), we obtain

$$\frac{\beta}{2} k_2 - 2 \left(1 - \frac{\beta}{2}\right) k_4 x = 0, \quad (55)$$

which, to leading order, yields

$$x_{\text{crit}} = \frac{k_2}{4k_4} \beta, \quad (56)$$

the exact same result (49) that we previously obtained in Approach I.

We can now insert equation (56) into equation (53) to obtain an expression for the change in the mass. We again use the expansion (50). Expanding the exponents in equation (53) to linear order, we find

$$\begin{aligned} \bar{M}^{-2/3 - \beta/3} &\simeq (\bar{M}_0^{\text{sph}})^{-2/3 - \beta/3} \left(1 - \frac{2}{3} \delta_{\text{M}}^{\text{sph}}\right) \quad (57) \\ &= (\bar{M}_0^{\text{sph}})^{-2/3} \exp\left(-\frac{\beta}{3} \ln \bar{M}_0^{\text{sph}}\right) \left(1 - \frac{2}{3} \delta_{\text{M}}^{\text{sph}}\right) \\ &\simeq (\bar{M}_0^{\text{sph}})^{-2/3} \left(1 - \frac{\beta}{3} \ln \bar{M}_0^{\text{sph}} - \frac{2}{3} \delta_{\text{M}}^{\text{sph}}\right) \end{aligned}$$

as well as

$$\begin{aligned}
 x^{\beta/2} &= \left(\frac{k_2}{4k_4} \beta \right)^{\beta/2} = \exp \left(\frac{\beta}{2} \ln \left(\frac{k_2}{4k_4} \right) \right) \exp \left(\frac{\beta}{2} \ln \beta \right) \quad (58) \\
 &\simeq 1 + \frac{\beta}{2} \ln \left(\frac{k_2}{4k_4} \right) + \frac{\beta}{2} \ln \beta.
 \end{aligned}$$

Inserting these expansions into equation (53) then yields

$$0 = k_1 (\bar{M}_0^{\text{sph}})^{-2/3} \left(1 + \frac{\beta}{2} - \frac{\beta}{3} \ln \bar{M}_0^{\text{sph}} - \frac{2}{3} \delta_M + \frac{\beta}{2} \ln \frac{k_2}{4k_4} + \frac{\beta}{2} \ln \beta \right) - k_2 - k_2 \frac{\beta}{2}, \quad (59)$$

Not surprisingly, this equation yields the Newtonian mass (39) to zeroth order. The next leading-order terms can be solved for δ_M^{sph} to yield

$$\delta_M^{\text{sph,II}} = \left(\frac{3}{4} \ln \frac{k_2}{4k_4} + \frac{3}{4} \ln \beta - \frac{1}{2} \ln \bar{M}_0^{\text{sph}} \right) \beta, \quad (60)$$

where we have used equation (39) to eliminate k_2 . This result is included in Fig. 2 as a dashed line. Note that this result is different from that obtained in Approach I, equation (51), as we will discuss in more detail in the following section.

3.3 Comparisons

Figs 1 and 2 show the numerical results of Section 3.1 and the analytical results of Section 3.2 for both Approaches I and II. We emphasize again that all calculations employed here, both numerical and analytical, treat the effects of gas pressure only approximately. Approach I is based on a Taylor expansion that approximates the total entropy s to be constant to leading-order only (see Section 2.4), while Approach II approximates the EOS as polytropic, leading to a polytropic constant that is only approximately constant (see Section 2.5). We believe that the nature of the approximation is more fundamental in Approach I. However, as we will discuss in more detail below, we find that both approaches make identical predictions for some key dimensionless quantities at the critical point.

We have already noted that Approaches I and II give identical results (49) and (56) for the dimensionless density variable x_{crit} ; the two lines representing these results therefore lie on top of each other in Fig. 1. In this figure, we see that this analytical prediction also agrees very well with the numerical results for both Approaches I and II, at least to leading order in β . Since all calculations included in the figure are accurate to leading-order only, the apparently better agreement between the analytical prediction and the numerical results for Approach II for larger β is presumably coincidental.

We already noted that Approaches I and II make different predictions for the change in the rescaled mass δ_M^{sph} ; see equations (51) and (60). In Fig. 2, we include the two predictions with a solid and dashed lines and find that, for small β , they each agree very well with the respective numerical results for Approaches I and II. In fact, it is not surprising that the two different approaches result in different values of \bar{M} , since the two different approaches adopt two different rescalings between \bar{M} and the physical mass M : In Approach I, we have $M = K_I^{3/2} \bar{M}$, and in Approach II, $M = K_{II}^{n_1/2} \bar{M}$. Even inserting the different constants K_I (21) and K_{II} (30) results in some ambiguities, since K_I assumes that the total entropy s_T is constant, while K_{II} depends on the radiation entropy s_r and, weakly, on the density ρ_0 . In order to avoid these ambiguities, we will therefore focus on dimensionless quantities that do not depend on K . We have already seen that both approaches make identical predictions for x_{crit} , which relates the central density ρ_0 to the stellar mass M . We will similarly see in Section 5 that, for rotating stars, both approaches also make identical predictions for the change in the dimensionless parameters that we are primarily interested in, namely the angular momentum $j_{\text{crit}} = (J/M^2)_{\text{crit}}$, and the compaction $(R/M)_{\text{crit}}$, both evaluated at the maximally rotating critical configuration.

For completeness, though, we also include in Fig. 2, the numerical results of SUS, who adopted Approach II to model the effects of gas pressure. Since SUS do not provide values for $\beta = 0$, i.e. $\Gamma = 4/3$, we extrapolate the numerical values \bar{M}^{sph} listed in their table 1 to $\beta = 0$, which yields their value of the Newtonian, spherical mass \bar{M}_0^{sph} . We then compute $\delta_M^{\text{sph}} = (\bar{M}^{\text{sph}} - \bar{M}_0^{\text{sph}})/\bar{M}_0^{\text{sph}}$. As expected, their values agree well with our numerical values for Approach II, and, for small β , both agree well with our analytical prediction for Approach II.

Finally, we demonstrate that our results reproduce those of ST, who adopt Approach I to compute the density of non-rotating SMSs in their Section 17.4, but use a different notation. Inserting the definition (34) into (49), we obtain

$$\rho_{\text{crit}} = \left(\frac{1}{4} \frac{k_2}{k_4}\right)^3 \frac{\beta^3}{M^2} = \left(\frac{8.5}{4} \frac{k_2 c^2}{k_4 G}\right)^3 \left(\frac{M_{\odot}}{M}\right)^{7/2} \frac{1}{M_{\odot}^2}, \quad (61)$$

where we have used the relation (40) in the last step, and where we have also inserted appropriate powers of c and G to obtain an expression in cgs units. Inserting values for the latter, as well as the solar mass M_{\odot} , we obtain

$$\rho_{\text{crit}} = 1.92 \times 10^{-3} \left(\frac{10^6 M_{\odot}}{M}\right)^{7/2} \frac{\text{g}}{\text{cm}^3}, \quad (62)$$

very similar to the value provided in equation (ST.17.4.7). Using $M = 4\pi\rho_{\text{ave}}R^3/3$ as well as $\rho_c/\rho_{\text{ave}} \simeq 54.18$ for an $n=3$ polytrope, we also have

$$\left(\frac{R}{M}\right)_{\text{crit}} = 1.59 \times 10^3 \left(\frac{M}{10^6 M_{\odot}}\right)^{1/2} \quad (63)$$

[compare equation (ST.17.4.11)]. Equation (62) gives the critical density for the onset of radial collapse of a spherical SMS with both radiation and gas pressure and equation (63) its value of R/M : stars with $\rho < \rho_{\text{crit}}$ and $R/M > (R/M)_{\text{crit}}$ are stable, while those with $\rho > \rho_{\text{crit}}$ and $R/M < (R/M)_{\text{crit}}$ are unstable to collapse.

4 PERTURBATIVE EFFECTS ON THE STABILITY OF ROTATING SMSS

In this section, we extend the analytical model of Section 3.2.1 to develop a general framework for treating perturbative effects on uniformly rotating SMSs. We first review the model and results obtained in Paper I for the critical configuration in the absence of other perturbations in Sections 4.1 and 4.2, and then introduce general expressions for perturbations of these critical solution in Section 4.3. We will leave the nature of the perturbation unspecified in this section. In Section 5, we will then apply this formalism to gas pressure and in Section 6 to other effects, all in the presence of rotation.

4.1 Review of the analytical model

In order to model rotating SMSs, we include in the energy functional (37) both a rotational energy term as well as a second post-Newtonian correction to the Newtonian potential energy,

$$E = k_1 K M \rho_c^{1/n} - k_2 M^{5/3} \rho_c^{1/3} + k_3 j^2 M^{7/3} \rho_c^{2/3} - k_4 M^{7/3} \rho_c^{2/3} - k_5 M^3 \rho_c \quad (64)$$

[see equation (20) in Paper I, hereafter equation (I.20)]. Here, $j = JM^2$ is a dimensionless measure of the angular momentum J , and the structure constants k_i are again listed in Table 1 for an $n = 3$ polytrope. As in Section 3.2, we will assume that these structure constants remain unchanged in all our perturbative calculations. Even though the second post-Newtonian correction, the last term in the above expression, takes a very small value, its inclusion is crucial for determining the critical configuration, i.e. the onset of instability (see Zeldovich & Novikov 1971, Paper I). Using the same dimensional rescaling as before, e.g. $\bar{M} \equiv K^{-n/2} M$ and $\bar{x} \equiv K^{-n/2} x$, as well as the definition (34), we can rewrite equation (64) as

$$\bar{E} = k_1 \bar{M}^{1-2/n} \bar{x}^{3/n} - k_2 \bar{M} \bar{x} + k_3 j^2 \bar{M} \bar{x}^2 - k_4 \bar{M} \bar{x}^2 - k_5 \bar{M} \bar{x}^3. \quad (65)$$

We note that in Paper I, we used the alternative scaling $\tilde{x} \equiv \bar{\rho}_c^{-1/3} = \bar{M}^{-2/3} x$ for $n=3$. The advantage of the scaling equation (34), $x = \bar{M}^{2/3} \bar{\rho}_c^{-1/3}$, is that the dimensionless mass \bar{M} now appears with the same power in all terms except in the first.

Equilibrium configurations can be found by setting to zero the derivative of the energy equation (65) with respect to x (at constant mass and angular momentum),

$$0 = \frac{\partial \bar{E}}{\partial x} = (3/n)k_1 \bar{M}^{1-2/n} x^{3/n-1} - k_2 \bar{M} + 2k_3 j^2 \bar{M} x - 2k_4 \bar{M} x - 3k_5 \bar{M} x^2. \quad (66)$$

The onset of instability occurs at turning points of the equilibrium sequences, i.e. at points at which the second derivative with respect to x vanishes,

$$0 = \frac{\partial^2 \bar{E}}{\partial x^2} = (3/n)(3/n-1)k_1 \bar{M}^{1-2/n} x^{3/n-2} + 2k_3 j^2 \bar{M} - 2k_4 \bar{M} - 6k_5 \bar{M} x. \quad (67)$$

For $n=3$, equations (66) and (67) are equivalent to equations (I.21) and (I.22).

The ratio between the rotational kinetic and Newtonian potential energies can be computed from the second and third terms in equation (64),

$$\frac{T}{|W|} = \frac{k_3 j^2 x}{k_2} \quad (68)$$

[compare equation (I.27)]. Adopting the Roche model, we can compute the rotational kinetic energy at mass shedding from $T = (1/2)I\Omega_{\text{shed}}^2$. Consistent with our assumption that the structure constants k_i remain unchanged, we will assume that the moment of inertia I always remains that of the non-rotating $n=3$ polytrope, $I \simeq (2/3)0.1130MR_p^2$ [see equation (I.18)], and where $\Omega_{\text{shed}} = (2/3)^{3/2}(M/R_p^3)^{1/2}$ [see equation (I.17)]. We similarly assume that the potential energy remains that of the non-rotating $n=3$ polytrope, $|W| = (3/2)M^2/R_p$. Combining these terms, we find

$$\left(\frac{T}{|W|}\right)_{\text{shed}} = 7.44 \times 10^{-3} \quad (69)$$

[see equation (I.19)], which can be inserted into equation (68) for a star uniformly rotating at mass shedding, the maximum spin rate. Note that the small value of $T/|W|$ at mass shedding

for an $n = 3$ polytope (due to its large central mass concentration) justifies ignoring changes in the shape of the bulk of the mass in computing the energy functional, and treating the star as spherical to lowest order.

Noting that we may also write the kinetic rotational energy as $T = (1/2)I\dot{\phi}^2$, we find

$$\frac{T}{|W|} = 4.425 \frac{M}{R_p} j^2, \quad (70)$$

which can then be inverted to yield an expression for the compaction R_p/M ,

$$\frac{R_p}{M} = 4.425 \frac{j^2}{T/|W|}. \quad (71)$$

Equations (66)–(68), with $T/|W|$ given by equation (69), now provide three equations for the three unknown parameters x , \bar{M} , and j describing the critical configuration of marginally stable SMSs rotating at mass shedding. In the following sections, we will solve these equations perturbatively, adopting as the unperturbed background solution the critical configuration of an $n = 3$ polytrope as derived in Paper I.

4.2 The unperturbed critical configuration

In Paper I, we solved equations (66)–(68) under the idealized assumption that the SMS is dominated by a radiation fluid, so that $n = 3$. In that case, equation (67) yields

$$x_0 = \frac{k_3 j_0^2 - k_4}{3k_5} \quad (72)$$

[compare equation (I.23)], where we have introduced the subscript ‘0’ to denote parameters describing the critical configuration of the unperturbed $n=3$ polytrope. As an immediate consequence, we see that rotation alone can stabilize the star only for angular momenta j_0 greater than a minimum angular momentum

$$j_{\min} = \left(\frac{k_4}{k_3} \right)^{1/2} = 0.8733. \quad (73)$$

Using this result, we can rewrite equation (72) as

$$x_0 = \frac{k_3}{3k_5}(j_0^2 - j_{\min}^2) \quad (74)$$

and equation (66) as

$$k_1 \bar{M}_0^{-2/3} = k_2 - 2k_3(j_0^2 - j_{\min}^2)x_0 + 3k_5x_0^2. \quad (75)$$

Inserting equation (74) into the latter then yields

$$\bar{M}_0^{2/3} = k_1 \left(k_2 - \frac{k_3}{3k_5}(j_0^2 - j_{\min}^2)^2 \right)^{-1} \quad (76)$$

[see equation (I.25)]. Inserting equation (74) into equation (68) results in a quadratic equation for j_0^2 ,

$$j_0^4 - j_{\min}^2 j_0^2 - \frac{3k_2 k_5}{k_3^2} \frac{T}{|W|} = 0, \quad (77)$$

which can be solved for j_0 as a function of $T/|W|$. This solution provides the dimensionless angular momentum of the critical configuration,

$$\left(\frac{J}{M^2} \right)_{\text{crit},0} = j_0 = 0.876. \quad (78)$$

Inserting j_0 together with equation (69) into equation (71), then yields

$$\left(\frac{R_p}{M} \right)_{\text{crit},0} \simeq 456 \quad (79)$$

for the analytical model. In the Roche model, the equatorial radius R_{eq} is related to the polar radius R_p by $R_{\text{eq}} = 3R_p/2$, hence

$$\left(\frac{R_{\text{eq}}}{M}\right)_{\text{crit},0} \simeq 684. \quad (80)$$

In addition to this analytical model calculation, we also performed a fully relativistic, numerical calculation in Paper I, which resulted in $j_0 \simeq 0.97$ and $R_p/M \simeq 427$. From equation (74) for x_0 , we also find the critical central density

$$\begin{aligned} \rho_{\text{crit},0} &= \left(\frac{c^2}{G}\right)^3 \frac{x_0^3}{M_\odot^2} \left(\frac{M_\odot}{M}\right)^2 \\ &= 8.7 \times 10^{-2} \left(\frac{10^6 M_\odot}{M}\right)^2 \frac{\text{g}}{\text{cm}^3}. \end{aligned} \quad (81)$$

Equations (79) and (81) should be compared with equations (63) and (62). The former two describe the physical properties of the critical configuration of an SMS star stabilized by uniform rotation, while the latter two describe those of the critical configuration of an SMS star stabilized by gas pressure.

In Table 2, we list some of the characteristic parameters of the unperturbed critical configuration, as found in Paper I from both the analytical model calculation and the numerical simulations (cf. table 2 in Paper I). We also include numerical values for j_0 and \bar{M}_0 as computed from the values provided by SUS. As discussed in Section 3.3, we compute these values by extrapolating the data listed in their table 1 to $n = 3$.

Equations (78) and (79) provide the unique parameters of the critical configuration of a uniformly rotating SMS, supported by pure radiation pressure and spinning at the mass-shedding limit. The subsequent gravitational collapse to a black hole is therefore also unique, up to the overall scaling with mass, and the emitted gravitational wave signal may hence serve as a ‘standard-siren’ for future space-based gravitational wave detectors. In the following sections, we will consider perturbations of these critical configurations in order to explore the regimes in which this universality is affected by the presence of gas pressure, magnetic fields, DM, and dark energy.

4.3 Perturbative treatment: general set-up

We will account for perturbations of the idealized assumptions of Section 4.2 (and Paper I) by including new terms in the energy functional (64). These terms therefore lead to perturbations in the variables that characterize the critical configuration, namely the density variable x , the angular momentum j , and mass \bar{M} , given by solutions to equations (66)–(68). In our perturbative approach, we write these deviations as

$$x = x_0(1 + \delta_x), \quad (82)$$

$$j = j_0(1 + \delta_j), \quad (83)$$

$$\bar{M} = \bar{M}_0(1 + \delta_M), \quad (84)$$

where x_0 , j_0 , and \bar{M}_0 are the unperturbed parameters of Section 4.2. We are assuming that the onset of instability is still dominated by the interplay between radiation pressure, rotation, and post-Newtonian corrections to the potential energy, as outlined in Section 4.1, and that all corrections (e.g. gas pressure in the limit $\beta \ll 1$) affect this onset of instability only perturbatively. Other approaches are possible, of course, but are not what we pursue in this paper.

Specific expressions for δ_x , δ_j , and δ_M will depend on the specific effects considered, and will be derived in the following sections. Equation (68), however, is independent of the energy function itself, and, thanks to our rescaling equation (34), also does not depend on \bar{M} . Assuming that $T/|W|$ remains given by equation (69), which is consistent with our assumption that the structure constants k_i remain unchanged, we may therefore insert both equations (82) and (83) into equation (68) and expand to linear order to obtain

$$\frac{T}{|W|} = \frac{k_3}{k_2} j_0^2 x_0 (1 + 2\delta_j + \delta_x). \quad (85)$$

Evidently, to linear order, we must always have

$$\delta_x = -2\delta_j. \quad (86)$$

We then insert equation (83) into equation (71) to obtain

$$\left(\frac{R_p}{M}\right)_{\text{crit}} = \left(\frac{R_p}{M}\right)_{\text{crit},0} (1 + 2\delta_j). \quad (87)$$

to linear order. From equation (83), we also have

$$\left(\frac{J}{M^2}\right)_{\text{crit}} = \left(\frac{J}{M^2}\right)_{\text{crit},0} (1 + \delta_j). \quad (88)$$

The above expressions can now be used to determine the change in the angular momentum j and the critical compaction R_p/M , once δ_x has been found.

5 EFFECTS OF GAS PRESSURE

In this section, we return to the effects of gas pressure, and consider its effect on the stability of maximally rotating SMSs using both Approaches I and II (Sections 5.1 and 5.2). We compare with the numerical results of SUS in Section 5.3, and evaluate our results to compute changes in the physical parameters of critically spinning SMSs in Section 5.4.

5.1 Approach I

Following Section 3.2.2, we account for gas pressure by adopting equation (65) with $n = 3$, as well as $K = K_I$ in the dimensional rescaling, but adding the correction (42) to the internal energy. The energy functional then becomes

$$\bar{E} = k_1 \bar{M}^{1/3} x + k_1 \bar{M}^{1/3} x \beta \left(\frac{1}{2} \ln x + \frac{5}{6} \ln \beta + C \right) - k_2 \bar{M} x + k_3 j^2 \bar{M} x^2 - k_4 \bar{M} x^2 - k_5 \bar{M} x^3, \quad (89)$$

where C is given by equation (43). Setting the first two derivatives to zero, we obtain

$$0 = k_1 \bar{M}^{2/3} k_1 \bar{M}^{-2/3} \beta \left(\frac{1}{2} \ln x + \frac{5}{6} \ln \beta + C \right) + \frac{1}{2} k_1 \bar{M}^{-2/3} - k_2 + 2k_3 j^2 x - 2k_4 x - 3k_5 x^2 \quad (90)$$

and

$$0 = \frac{1}{2} k_1 \bar{M}^{-2/3} \beta x^{-1} + 2k_3 j^2 - 2k_4 - 6k_5 x. \quad (91)$$

We now insert equations (82) and (83) into equation (91) to find, to leading order,

$$0 = \frac{1}{2} \bar{M}_0^{-2/3} x_0^{-1} \beta + 2k_3 j_0^2 (1 + 2\delta_j) - 2k_3 j_{\text{min}}^2 - 6k_5 x_0 (1 + \delta_x), \quad (92)$$

where we have used equation (73). Not surprisingly, the zeroth-order term gives us equation (74) again. Using equation (86), the linear terms can be solved to yield an expression for the change in j ,

$$\delta_j = -\frac{k_1}{8k_3} \frac{1}{\bar{M}_0^{2/3} (2j_0^2 - j_{\min}^2) x_0} \beta. \quad (93)$$

This expression can be inserted into equations (87) and (88) to find a change in the dimensional parameters R_p/M and JM^2 – the quantities that we are primarily interested in. We will postpone a discussion of these results, though, until Section 5.3. The change in the density variable x can also be found from equation (93) with the help of equation (86).

Keeping in mind the discussion of δ_M in Section 3.3, we can compute this quantity as follows. We first insert equation (91) into equation (90) to obtain

$$0 = k_1 \bar{M}^{-2/3} + k_1 \bar{M}^{-2/3} \beta \left(\frac{1}{2} \ln x + \frac{5}{6} \ln \beta + C \right) - k_2 + 3k_5 x^2. \quad (94)$$

We then insert equations (82) and (84) and expand to linear order, which yields

$$\delta_M^I = \left(\frac{3}{4} \ln x_0 + \frac{5}{4} \ln \beta + \frac{3}{2} C \right) \beta + \frac{9k_5 \bar{M}_0^{2/3} x_0^2}{k_1} \delta_x, \quad (95)$$

or, with equations (86) and (93),

$$\delta_M^I = \left(\frac{3}{4} \ln x_0 + \frac{5}{4} \ln \beta + \frac{3}{2} C + \frac{9k_5}{4k_3} \frac{x_0}{2j_0^2 - j_{\min}^2} \right) \beta. \quad (96)$$

Here, we have introduced a superscript ‘I’ in order to distinguish this result from the corresponding result (105) in Approach II. We will again postpone a discussion until after we have presented results for Approach II in the next sections.

5.2 Approach II

As in Section 3.2.3, we now account for gas pressure by adopting the approximate polytropic index $n = n_1$ as given by equation (32), using $K = K_{II}$ (approximated as a constant) in the dimensional rescaling. The first two derivatives (66) and (67) of the energy function (65) can then be written as

$$0 = \left(1 + \frac{\beta}{2} \right) k_1 \bar{M}^{-2/3 - \beta/3} x^{\beta/2} - k_2 + 2k_3 (j^2 - j_{\min}^2) x - 3k_5 x^2 \quad (97)$$

and

$$0 = \left(1 + \frac{\beta}{2}\right) \frac{\beta}{2} k_1 \bar{M}^{-2/3 - \beta/3} x^{\beta/2 - 1} + 2k_3(j^2 - j_{\min}^2) - 6k_5x, \quad (98)$$

where we have used equation (73). These two equations can then be combined to eliminate the first terms, leading to

$$\frac{\beta}{2} k_2 + 2 \left(1 - \frac{\beta}{2}\right) k_3(j^2 - j_{\min}^2)x - 6 \left(1 - \frac{\beta}{4}\right) k_5x^2 = 0. \quad (99)$$

Inserting equations (82) and (83), the leading-order correction terms become

$$0 = \frac{\beta}{2} k_2 + 2k_3j_0^2x_0 \left(2\delta_j + \delta_x - \frac{\beta}{2}\right) - 2k_3j_{\min}^2x_0 \left(\delta_x - \frac{\beta}{2}\right) - 6k_5x_0^2 \left(2\delta_x - \frac{\beta}{4}\right). \quad (100)$$

We now use equation (86) to eliminate δ_x and obtain

$$(4k_3j_{\min}^2x_0 + 24k_5x_0^2) \delta_j = \left(-\frac{1}{2}k_2 + k_3(j_0^2 - j_{\min}^2)x_0 - \frac{3}{2}k_5x_0^2\right) \beta. \quad (101)$$

Simplifying the left-hand side with equation (74), and the right-hand side with equation (75) yields the result

$$\delta_j = -\frac{k_1}{8k_3} \frac{1}{\bar{M}_0^{2/3} (2j_0^2 - j_{\min}^2)x_0} \beta, \quad (102)$$

which is identical to the result (93) that we found for Approach I. In particular, this means that both approaches predict identical changes in the parameters R_p/M and J/M^2 of the critical configuration, see equations (87) and (88), as well as for δ_x , see equation (86).

In order to obtain an expression for the correction δ_M of the rescaled mass \bar{M} , we expand equation (97). For the expansion of the mass term $\bar{M}^{-2/3 - \beta/3}$, we can use the expansion (57), but, unlike in equation (58), we now expand x about x_0 rather than zero, so we now have

$$x^{\beta/2} = e^{(\beta/2)\ln x} = 1 + \frac{\beta}{2} \ln x_0 \quad (103)$$

to linear order. Inserting these, together with equations (82) and (83), into equation (97) then yields

$$0 = k_1 \bar{M}_0^{-2/3} \left(1 + \frac{\beta}{2} - \frac{\beta}{3} \ln \bar{M}_0 + \frac{\beta}{2} \ln x_0 - \frac{2}{3} \delta_M \right) - k_2 + 2k_3 j_0^2 x_0 (1 + 2\delta_j + \delta_x) - 2k_3 j_{\min}^2 x_0 (1 + \delta_x) - 3k_5 x_0^2 (1 + 2\delta_x). \quad (104)$$

Not surprisingly, the zeroth-order terms reproduce equation (75). The leading-order correction terms can be simplified by using equation (86) to write δ_x in terms of δ_j , and equation (102) to write δ_j in terms of β . Also using equation (74), we then find

$$\delta_M^{\text{II}} = \left(\frac{3}{4} - \frac{1}{2} \ln \bar{M}_0 + \frac{3}{4} \ln x_0 - \frac{3}{4} \frac{j_0^2}{2j_0^2 - j_{\min}^2} \right) \beta. \quad (105)$$

Given our discussion in Section 3.3, it is not surprising that this result is not identical with that found for Approach I, equation (96).

5.3 Comparisons

It is useful to compare the above results with the numerical results of SUS, who adopted Approach II to study the effect of gas pressure on relativistic, maximally rotating SMSs. Since SUS do not provide results for $\beta = 0$, we extrapolate their numerical values for $\beta > 0$, listed in their table 1, to $\beta = 0$. The resulting values for j_0 and \bar{M}_0 are listed in our Table 2.

It is evident from Table 2 that the parameters describing the critical configurations show some variation between the different methods. We did not extract x_0 and j_{\min} from SUS, but these values agree reasonably well between the analytical and numerical approaches of Paper I. The largest difference appears for j_0 , and we note that the value obtained from SUS lies between the two values from Paper I. All of the above parameters, as well as \bar{M}_0 , appear in the expressions (93) for δ_j and expressions (96) and (105) for δ_M . Not surprisingly, these perturbations then depend on which background values are adopted. In Table 3, we list the ratios δ_j/β , δ_x/β , and $\delta_M^{\text{II}}/\beta$, using the different values of the background parameters (because of the appearance of the $\beta \ln \beta$ term in δ_M^{I} , the ratio $\delta_M^{\text{I}}/\beta$ is not independent of β ; we therefore omitted this quantity in the table). For the top two rows in the Table 3, we used the analytical and numerical values from Paper I for all four parameters x_0 , j_{\min} , j_0 , and \bar{M}_0 (i.e. the values from the corresponding top two rows in Table 2), while for the bottom entries, we used the extrapolated values from SUS for j_0 and \bar{M}_0 , but the numerical values of Paper I for x_0 and j_{\min} .

For δ_j/β in equation (102) (and similarly for δ_x/β), we find variations of several 10 per cent; these variations are mostly due to differences in the term $2j_0^2 - j_{\min}^2$ between the different approaches. Similar differences in equation (105) tend to cancel each other out, so that the numerical values for $\delta_M^{\text{II}}/\beta$ as obtained from different background values agree much better with each other. We believe that the high-resolution results of SUS provide the most accurate values currently available, and therefore will adopt their parameters in Section 5.4 below.

We next compare our predictions for δ_j and δ_M with the numerical results of SUS. In order to make this comparison, we compute $\delta_j = (j - j_0)/j_0$ (and similar for δ_M) from the data j listed in table 1 of SUS, where j_0 is the extrapolated value for $\beta = 0$ as listed in our Table 2. We also compute values for β from $\beta = 6 (\Gamma - 4/3)$, where the values of Γ are listed in table 1 of SUS. In Fig. 3, we then graph the numerical values of SUS for δ_j and δ_M as squares, and our perturbative results (93) as well as (96) and (105) as solid and dashed lines.

We first observe again that Approaches I and II make identical predictions for δ_j ; they therefore appear as a single line in the top panel of Fig. 3. Moreover, for small values of β , the perturbative predictions for δ_j agree well with the numerical results of SUS. For larger values of β , we see increasing deviations. This is not surprising, however, since, for the larger values of β adopted by SUS, our perturbative calculation predicts values of δ_j of order unity, which is clearly a violation of the condition $|\delta_j| \ll 1$ for a linear treatment [see equation (83)]. Another reason for these deviations at larger β may also be related to $T|W|$, which we assume to remain given by the constant Roche-approximation value (69) independently of β . The numerical simulations of SUS show, however, that instead $T|W|$, which is small, slightly increases with increasing β . This means that our approximation underestimates the angular momentum, increasing the deviation in δ_j .

Keeping in mind the subtleties discussed in Section 3.3, we also compare our predictions for δ_M in the lower panel of Fig. 3. The two different predictions from Approaches I and II are included as a solid and a dashed line; as in Fig. 2 for non-rotating SMSs Approach I predicts larger decreases in \bar{M} than Approach II. Quite reassuringly, but not surprisingly, Approach II agrees quite well with the results of SUS, who also adopt Approach II. In fact, for large β , this agreement is significantly better than for δ_j . In part, this is because δ_M is smaller in magnitude than δ_j for a given value of β , so that the linearity condition $|\delta_M| \ll 1$ is not violated as severely as the one for δ_j . We further expect that δ_M is less affected than δ_j by our approximation of keeping $T|W|$ constant, as we discussed above.

5.4 Results for physical parameters

Encouraged by the comparisons in the previous section, we now evaluate our perturbative results to compute the changes due to gas pressure in the physical parameters of the critical configuration of an SMS spinning at mass shedding. Inserting equation (93) together with equation (40) into equation (83), we find

$$\left(\frac{J}{M^2}\right)_{\text{crit}} \simeq \left(\frac{J}{M^2}\right)_{\text{crit},0} \left(1 - 0.12 \left(\frac{M}{10^6 M_{\odot}}\right)^{-1/2}\right) \quad (106)$$

and similarly, from equation (87),

$$\left(\frac{R_p}{M}\right)_{\text{crit}} \simeq \left(\frac{R_p}{M}\right)_{\text{crit},0} \left(1 - 0.23 \left(\frac{M}{10^6 M_{\odot}}\right)^{-1/2}\right), \quad (107)$$

where the unperturbed critical ratios are given in equations (78) and (79). Allowing for gas pressure has a stabilizing effect, permitting SMSs to remain stable to smaller values of R_p/M and higher densities. For stars with masses $M \lesssim 10^6 M_{\odot}$, the effect is quite substantial. In fact, for smaller stars gas pressure dominates the stabilization, as calculated in Section 3, and rotation should be treated as a perturbation, rather than the other way around as in this section.

To find the central density, we start with equation (34) to find

$$\rho_{\text{crit}} = \frac{x^3}{M^2} \simeq \left(\frac{c^2}{G}\right)^3 \frac{x_0}{M_{\odot}^2} \left(\frac{M_{\odot}}{M}\right)^2 (1 + 3\delta_x), \quad (108)$$

where we have inserted appropriate powers of c and G . Using equation (86) together with equation (40) and evaluating the physical constants, we now obtain,

$$\rho_{\text{crit}} \sim \rho_{\text{crit},0} \left(1 + 0.70 \left(\frac{M}{10^6 M_{\odot}}\right)^{-1/2}\right) \quad (109)$$

where $\rho_{\text{crit},0}$ is given by equation (81).

Equation (109) generalizes the earlier result (62), while equation (62) determines the effect of gas pressure on the critical density of a non-rotating SMS, equation (109) determines the density of a maximally rotating SMS at the onset of instability, allowing for gas pressure as a perturbation. The two expressions (62) and (109) scale differently with the mass M , which is related to the fact that they are based on different expansions. Equation (109) is the result of a perturbation about the non-zero critical density of the maximally spinning SMS. By contrast, in the absence of rotation, there is no stable configuration without gas pressure, so that, in deriving equation (62), there is no non-zero background critical density about which to expand.

We note again that the results (106), (107), and (109) follow identically from Approaches I and II.

6 OTHER EFFECTS

In this section, we adopt our perturbative approach to estimate the influence of several effects other than gas pressure on the radial stability of uniformly rotating SMSs at the mass-shedding limit.

6.1 Magnetic fields

We now consider the perturbative role of a magnetic field B , which we assume to be sufficiently weak so that the shape of the star remains unchanged and nearly spherical as in Section 4. This assumption requires that $E_M/W \ll 1$, where E_M is the total magnetic energy. The energy density of the magnetic field B is

$$\varepsilon_M = \frac{B^2}{8\pi}. \quad (110)$$

Integrating this energy density of all space gives a result that depends on the topology of the magnetic field. Typically, we find

$$E_M = k_M \Phi_M^2 M^{-1/3} \rho_c^{1/3}. \quad (111)$$

Here, we have expressed the magnetic field in terms of the magnetic flux Φ_M through the matter, which remains constant for a frozen-in magnetic field when we vary the stellar density ρ_0 . The constant k_M is a dimensionless quantity that depends on the topology of the magnetic field. For example, for the model considered by Spitzer (1978, p. 242), which consists of a constant interior field B and a root-mean-square exterior field that falls off as $B(R/r)^3$, we have

$$k_M = \left(\frac{4}{81\pi^5 C} \right)^{1/3} \quad (112)$$

where $C = \rho_c / \langle \rho \rangle \approx 54.18$ measures the central condensation of an $n = 3$ polytope, and where $\Phi_M = \pi B R^2$ is the flux through the equatorial plane of the star.

Using equation (34) and rescaling all dimensional quantities as before, including $\bar{\Phi}_M = K^{-3/2} \Phi_M$, we can rewrite equation (111) in the non-dimensional form

$$\bar{E}_M = k_M \bar{\Phi}_M^2 \bar{M}^{-1} x. \quad (113)$$

We now add equation (113) to the energy equation (65) to find the total energy

$$\bar{E} = k_1 \bar{M}^{1/3} x + k_M \bar{\Phi}_M^2 \bar{M}^{-1} x - k_2 \bar{M} x + k_3 j^2 \bar{M} x^2 - k_4 \bar{M} x^2 - k_5 \bar{M} x^3. \quad (114)$$

Setting the first two derivatives to zero yields

$$0 = \frac{\partial \bar{E}}{\partial x} = k_1 \bar{M}^{1/3} + k_M \bar{\Phi}_M^2 \bar{M}^{-1} - k_2 \bar{M} + 2k_3 j^2 \bar{M} x - 2k_4 \bar{M} x - 3k_5 \bar{M} x^2. \quad (115)$$

and

$$0 = \frac{\partial^2 \bar{E}}{\partial x^2} = 2k_3 j^2 \bar{M} - 2k_4 \bar{M} - 6k_5 \bar{M} x. \quad (116)$$

Since the magnetic contribution is proportional to x , like the internal energy and the Newtonian gravitational potential energy terms, the second derivative of the energy equation (114) with respect to x yields the same equation as equation (67) for $n = 3$. As a consequence, equations (72)–(74) and (77) also remain unchanged. Solving equation (77), again using equation (69), yields the same values for j_0 and x_0 . Therefore, the onset of instability occurs at the same values of both J/M^2 and R_p/M as in the unperturbed configuration,

$$\left(\frac{J}{M^2} \right)_{\text{crit}} = \left(\frac{J}{M^2} \right)_{\text{crit},0} \quad (117)$$

and

$$\left(\frac{R_p}{M} \right)_{\text{crit}} = \left(\frac{R_p}{M} \right)_{\text{crit},0}, \quad (118)$$

where the background values are again given in Section 4.2. The sole role of the magnetic perturbation in this approximation is to increase the mass slightly at a given central density, as a result of the magnetic term in equation (115), but this does not influence the radial

instability. The onset of instability is determined by the competition between rotation and relativistic gravitation, whereas the internal energy, Newtonian gravitational potential energy, and magnetic energy establish equilibrium, but are neutral with respect to stability.

We note that in the case of non-rotating SMSs, the magnetic field can lead to a significant increase in the stellar radius of equilibrium configurations (see Ostriker & Hartwick 1968, as well as section 7.2 in ST).

6.2 Dark matter

We start by considering the effects of a DM halo. We treat cold dark matter (CDM) and hot dark matter (HDM) separately, adopting the crude approximations developed in Appendix A. As shown in the appendix, the key parameter that distinguishes these two regimes is $2\Phi_{\text{SMS}}/v_{\infty}^2$, where Φ_{SMS} is the central potential of the SMS, and v_{∞} is the speed of the DM particles far from the SMS. We refer to the limit $2\Phi_{\text{SMS}}/v_{\infty}^2 \gg 1$ as CDM, and the limit $2\Phi_{\text{SMS}}/v_{\infty}^2 \ll 1$ as HDM. During its evolution the SMS cools and contracts and Φ_{SMS} increases. Likewise, during its evolution the Universe expands and v_{∞} decreases. Therefore, SMSs may reside in different regimes during different parts of their evolution and different epochs of the Universe. For example, SMSs arriving at the mass-shedding limit at the current cosmological epoch obey the CDM limit, as we show below, while SMSs arriving at the mass-shedding limit sufficiently early in the Universe, when $v_{\infty} \approx 1$, are in the HDM limit.

Approximating Φ_{SMS} as M/R and evaluating this quantity for the critical configuration at the mass-shedding limit, $M/R_p \approx 1/427$ (see Section 4.2), we find

$$\frac{2\Phi_{\text{SMS}}}{v_{\infty}^2} \simeq 4.68 \times 10^3 \left(\frac{v_{\infty}}{300 \text{ km s}^{-1}} \right)^{-2} \quad (119)$$

where we have normalized to a typical galactic DM speed, appropriate for low redshifts. In the current cosmological epoch, SMSs therefore reach their critical configuration in the CDM limit, where the above ratio is much greater than unity.

6.2.1 Cold dark matter—As we argued in Appendix A1, the energy contribution due to a CDM halo can be approximated by the term (A11),

$$\bar{E}_{\text{DM}} = k_{\text{CDM}} x_{\text{DM}}^3 v_{\infty}^{-1} \bar{M}^{-1/2} x^{-3/2}. \quad (120)$$

where $x_{\text{DM}} = M^{2/3} (\rho_{\text{DM}}^{\infty})^{1/3}$. Including equation (120) in the energy equation (65) and taking the first two derivatives then results in

$$0 = k_1 \bar{M}^{1/3} - k_2 \bar{M} + 2k_3(j^2 - j_{\min}^2) \bar{M} x - 3k_5 \bar{M} x^2 - \frac{3}{2} k_{\text{CDM}} x_{\text{DM}}^3 v_{\infty}^{-1} \bar{M}^{-1/2} x^{-5/2} \quad (121)$$

and

$$0 = 2k_3(j^2 - j_{\min}^2) \bar{M} - 6k_5 \bar{M} x + \frac{15}{4} k_{\text{CDM}} x_{\text{DM}}^3 v_{\infty}^{-1} \bar{M}^{-1/2} x^{-7/2}. \quad (122)$$

Dividing equation (122) by \bar{M} , multiplying by x [so that, to leading order, the perturbation of $j^2 x = j_0^2 x_0 (1 + 2\delta_j + \delta_x)$ vanishes according to equation (86)], and inserting the perturbations (82) and (83), we obtain

$$2k_3 j_0^2 x_0 - 2k_3 j_{\min}^2 x_0 (1 + \delta_x) - 6k_5 x_0^2 (1 + 2\delta_x) = -\frac{15}{4} k_{\text{CDM}} x_{\text{DM}}^3 v_{\infty}^{-1} \bar{M}_0^{-3/2} x_0^{-5/2}. \quad (123)$$

Since the DM perturbations scale with x_{DM}^3 , the term on the right-hand side is small already, and we can neglect the perturbations of \bar{M} and x in this term. The zeroth-order terms yield equation (74), while the leading-order corrections give

$$(k_3 j_{\min}^2 + 6k_5 x_0) \delta_x = \frac{15}{8} k_{\text{CDM}} x_{\text{DM}}^3 v_{\infty}^{-1} \bar{M}_0^{-3/2} x_0^{-7/2}. \quad (124)$$

We now use equations (74) and (86) to rewrite the term on the left-hand side to obtain

$$\delta_j = -\frac{15}{16} \frac{k_{\text{CDM}}}{k_3 \bar{M}_0^{3/2} x_0^{7/2} (2j_0^2 - j_{\min}^2)} \frac{x_{\text{DM}}^3}{v_{\infty}}. \quad (125)$$

or

$$\delta_j = -2.5 \times 10^8 \frac{G^3 M^2 \rho_{\text{DM}}^{\infty}}{c^5 v_{\infty}}, \quad (126)$$

where we have inserted the background values of Section 4.2 as discussed in Section 5.3. From equation (83), we then have

$$\left(\frac{J}{M^2}\right)_{\text{crit}} = \left(\frac{J}{M^2}\right)_{\text{crit},0} \times \left(1 - 4.1 \times 10^{-20} \left(\frac{M}{10^6 M_\odot}\right)^2 \left(\frac{\rho_{\text{DM}}^\infty}{10^{-25} \text{ g cm}^{-3}}\right) \left(\frac{v_\infty}{300 \text{ km s}^{-1}}\right)^{-1}\right), \quad (127)$$

and from equation (87)

$$\left(\frac{R_p}{M}\right)_{\text{crit}} = \left(\frac{R_p}{M}\right)_{\text{crit},0} \times \left(1 - 8.2 \times 10^{-20} \left(\frac{M}{10^6 M_\odot}\right)^2 \left(\frac{\rho_{\text{DM}}^\infty}{10^{-25} \text{ g cm}^{-3}}\right) \left(\frac{v_\infty}{300 \text{ km s}^{-1}}\right)^{-1}\right), \quad (128)$$

where the unperturbed values are given by equations (78) and (79). Here, we have adopted values for the DM density and DM particle speeds as they may exist in current DM haloes. Evidently, the effects of such a CDM halo on the stability of rotating SMSs are minute.

6.2.2 Hot dark matter—In order to account for the effects of an HDM halo on the stability of rotating SMSs, we add the expression (A17),

$$\bar{E}_{\text{DM}} = k_{\text{HDM}} \bar{M}^{-2/3} x_{\text{DM}}^3 x^{-2}, \quad (129)$$

to the energy functional equation (65), where we have again defined $x_{\text{DM}} = M^{2/3} (\rho_{\text{DM}}^\infty)^{1/3}$.

The first two derivatives of the energy equation (65) are then

$$0 = k_1 \bar{M}^{1/3} - k_2 \bar{M} + 2k_3 (j^2 - j_{\text{min}}^2) \bar{M} x - 3k_5 \bar{M} x^2 - 2k_{\text{HDM}} x_{\text{DM}}^3 \bar{M}^{-2/3} x^{-3} \quad (130)$$

and

$$0 = 2k_3 (j^2 - j_{\text{min}}^2) \bar{M} - 6k_5 \bar{M} x + 6k_{\text{HDM}} x_{\text{DM}}^3 \bar{M}^{-2/3} x^{-4} \quad (131)$$

As in Section 6.2.1, we multiply equation (131) with x , divide by \bar{M} , perturb about the background solution of Section 4.2, and keep the leading-order correction terms to obtain

$$0 = -2k_3 j_{\text{min}}^2 x_0 \delta_x - 12k_5 x_0^2 \delta_x + 6k_{\text{HDM}} x_{\text{DM}}^3 \bar{M}_0^{-5/3} x_0^{-3} \quad (132)$$

(where again all corrections scale with x_{DM}^3 , so that this term is a small quantity already.)

Using equation (86) as well as equation (74), we may rewrite this expression as

$$\delta_j = -\frac{3}{2} \frac{k_{\text{HDM}} \bar{M}_0^{-5/3} x_{\text{DM}}^3}{k_3(2j_0^2 - j_{\text{min}}^2) x_0^4}. \quad (133)$$

or

$$\delta_j = -\frac{3}{2} \frac{k_{\text{HDM}} \bar{M}_0^{-5/3}}{k_3(2j_0^2 - j_{\text{min}}^2) x_0^4} \left(\frac{G}{c^2}\right)^3 M^2 \rho_{\text{DM}}. \quad (134)$$

Evaluating the background quantities as discussed in Section 5.3 and inserting into equation (83), we find

$$\left(\frac{J}{M^2}\right)_{\text{crit}} \simeq \left(\frac{J}{M^2}\right)_{\text{crit},0} \times \left(1 - 0.038 \left(\frac{M}{10^6 M_\odot}\right)^2 \left(\frac{\rho_{\text{DM}}}{10^{-5} \text{ g cm}^{-3}}\right)\right), \quad (135)$$

where we followed McLaughlin & Fuller (1996) and Bisnovatyi-Kogan (1998) in adopting a DM density of $10^{-5} \text{ g cm}^{-3}$, appropriate for some epoch in the early Universe. Inserting equation (134) into equation (87), we also find

$$\left(\frac{R_p}{M}\right)_{\text{crit}} \simeq \left(\frac{R_p}{M}\right)_{\text{crit},0} \times \left(1 - 0.077 \left(\frac{M}{10^6 M_\odot}\right)^2 \left(\frac{\rho_{\text{DM}}}{10^{-5} \text{ g cm}^{-3}}\right)\right). \quad (136)$$

Even for a large value of the DM density, the effect of the DM on the critical configuration of uniformly rotating SMSs is relatively small unless $M > 10^6 M_\odot$, which is consistent with the findings of McLaughlin & Fuller (1996) and Bisnovatyi-Kogan (1998).

6.3 Dark energy

The effects of a cosmological constant can be estimated very similarly to that of constant DM density distribution in the HDM regime. The Newtonian limit of *Einstein's* equations, including a cosmological constant Λ , is

$$\nabla^2 \Phi = 4\pi\rho - \Lambda. \quad (137)$$

We can therefore find the effects of the cosmological constant simply by replacing the constant value of ρ_{HDM} in the equations of Section 6.2.2 with $-\Lambda/(4\pi)$. Making this replacement in equation (134) and inserting physical constants, we find

$$\delta_j = \frac{3}{8\pi} \frac{k_{\text{HDM}}}{k_3} \frac{1}{\bar{M}_0^{5/3} (2j_0^2 - j_{\text{min}}^2) x_0^4} \left(\frac{G}{c^2}\right)^2 M^2 \Lambda. \quad (138)$$

Evaluating the coefficients using the background quantities of Section 4.2 and inserting into equation (83), we find

$$\left(\frac{J}{M^2}\right)_{\text{crit}} \simeq \left(\frac{J}{M^2}\right)_{\text{crit},0} \times \left(1 + 4.5 \times 10^{-26} \left(\frac{M}{10^6 M_\odot}\right)^2 \left(\frac{\Lambda}{\Lambda_{\text{SM}}}\right)\right), \quad (139)$$

where we have adopted

$$\Lambda_{\text{SM}} = 1.11 \times 10^{-56} \text{ cm}^{-2} \quad (140)$$

for the cosmological constant in the standard model (Planck Collaboration XIII 2016). Inserting equation (138) into (87), we similarly obtain

$$\left(\frac{R_p}{M}\right)_{\text{crit}} \simeq \left(\frac{R_p}{M}\right)_{\text{crit},0} \times \left(1 + 0.91 \times 10^{-25} \left(\frac{M}{10^6 M_\odot}\right)^2 \left(\frac{\Lambda}{\Lambda_{\text{SM}}}\right)\right). \quad (141)$$

Evidently, the effects of the dark energy on the stability of typical SMSs are entirely negligible.

7 SUMMARY

In this paper, we extend a calculation initiated in Paper I, where we determined the critical configuration at the onset of collapse of a uniformly rotating SMS, supported by pure radiation pressure and spinning at the mass-shedding limit. We found that this critical configuration is characterized by a unique set of the non-dimensional parameters R_p/M and J/M^2 .

In this case, the subsequent collapse of the critical configuration follows a universal evolutionary track and results in a spinning black hole with $M_{\text{BH}}/M \approx 0.9$ and $J_{\text{BH}}/M_{\text{BH}}^2 \approx 0.7$ (Shibata & Shapiro 2002; Shapiro & Shibata 2002), surrounded by a disc with $M_{\text{disc}}/M \approx 0.1$. Moreover, if the initial star is threaded by a weak, toroidal magnetic field, then the black hole–disc system launches a jet, and the electromagnetic Poynting luminosity transported by the jet resides in a narrow range of $L_{\text{EM}} \approx 10^{52 \pm 1} \text{ erg s}^{-1}$, independent of mass, once the system settles into quasi-steady accretion (see Sun et al.

2017; Shapiro 2017). The universal evolutionary track also leads to the emission of a universal gravitational signal (Shibata et al. 2016a; Sun et al. 2017), which may serve as a ‘standard siren’ for future space-based gravitational wave detectors.

In this paper, we explore the domain of validity of this universality by considering a number of different physical effects that might perturb this rotating critical configuration. In particular, we study the effects of gas pressure, magnetic fields, DM, and dark energy, and find that they perturb the critical parameters J/M^2 and R/M according to

$$\left(\frac{J}{M^2}\right)_{\text{crit}} \simeq \left(\frac{J}{M^2}\right)_{\text{crit},0} \left(1 - 0.12 \left(\frac{M}{10^6 M_\odot}\right)^{-1/2} - 4.1 \times 10^{-20} \left(\frac{M}{10^6 M_\odot}\right)^2 \left(\frac{\rho_{\text{DM}}}{10^{-25} \text{ g cm}^{-3}}\right) \left(\frac{v_\infty}{300 \text{ km s}^{-1}}\right)^{-1} + 4.5 \times 10^{-26} \left(\frac{M}{10^6 M_\odot}\right)^2 \left(\frac{\Lambda}{\Lambda_{\text{SM}}}\right)\right), \quad (142)$$

and

$$\left(\frac{R_p}{M}\right)_{\text{crit}} \simeq \left(\frac{R_p}{M}\right)_{\text{crit},0} \left(1 - 0.23 \left(\frac{M}{10^6 M_\odot}\right)^{-1/2} - 8.2 \times 10^{-20} \left(\frac{M}{10^6 M_\odot}\right)^2 \left(\frac{\rho_{\text{DM}}}{10^{-25} \text{ g cm}^{-3}}\right) \left(\frac{v_\infty}{300 \text{ km s}^{-1}}\right)^{-1} + 0.91 \times 10^{-25} \left(\frac{M}{10^6 M_\odot}\right)^2 \left(\frac{\Lambda}{\Lambda_{\text{SM}}}\right)\right), \quad (143)$$

where the unperturbed values are given by equations (78) and (79).

Gas pressure is the most significant perturbation for the most realistic astrophysical scenarios, and becomes important for SMSs with masses of $M \lesssim 10^6 M_\odot$. Its effects are accounted for by the top lines in equations (142) and (143). We model these effects using two different approaches (see Sections 2.4 and 2.5), which we carefully compare and calibrate (see Section 3). Both approaches lead to identical results for the leading-order effects on J/M^2 and R/M , which also agree well with the numerical results of SUS in the linear regime. Gas pressure has a stabilizing effect on rotating SMSs, it scales with $M^{-1/2}$ and becomes important for $M \lesssim 10^6 M_\odot$.

It turns out that magnetic fields have an effect on the mass of the critical configuration of maximally rotating SMSs, but not on the dimensionless ratios J/M^2 and R_p/M – the effect of magnetic fields is therefore absent in equations (142) and (143).

We approximate the effects of a DM halo adopting two opposite limiting cases, which we refer to as CDM and HDM. Rotating SMSs that reach the onset of instability in the current

cosmological epoch are in the CDM regime, which we include in the middle lines of equations (142) and (143). The effects of DM are stabilizing, but are minute and can be neglected for most situations. For SMSs forming in the early universe, the HDM regime may apply; the result, rescaled for a higher DM density as it might have applied in the early Universe, can be found in equations (135) and (136).

Finally, the effects of dark energy are included in the last lines of equations (142) and (143); these effects are destabilizing but even smaller than those for of a DM halo.

In general relativity, SMSs supported by angular momentum and pure radiation pressure can be stabilized against collapse only for angular momenta j that are greater than j_{\min} defined in equation (73), which is close to the mass-shedding value (78). Thus, for our perturbative calculations, which take configurations stabilized by rotation and radiation pressure as background models, slowly rotating stars as described by, e.g. Maeder & Meynet (2000), Yoon, Kang & Kozyreva (2015), and Haemmerlé et al. (2018b), are not suitable. SMSs that are rotating well below the mass-shedding limit could be modelled as configurations in which gas pressure plays the dominant stabilizing role and rotation is a small perturbation – but these are not the configurations that we focus on in this paper.

Acknowledgments

SPB and ARL gratefully acknowledge support through undergraduate research fellowships at Bowdoin College. This work was supported in part by NSF grants PHY-1402780 and PHY-1707526 to Bowdoin College, as well as NSF grants PHY-1602536 and PHY-1662211 and NASA grants NNX13AH44G and 80NSSC17K0070 to the University of Illinois at Urbana-Champaign (UIUC). TWB would like to thank UIUC for extending their hospitality during a visit.

References

- Agarwal B, Khochfar S, Johnson JL, Neistein E, Dalla Vecchia C, Livio M. MNRAS. 2012; 425:2854.
- Agarwal B, Johnson JL, Zackrisson E, Labbe I, van den Bosch FC, Natarajan P, Khochfar S. MNRAS. 2016; 460:4003.
- Agarwal B, Johnson JL, Khochfar S, Pellegrini E, Rydberg C-E, Klessen RS, Oesch P. MNRAS. 2017; 469:231.
- Alvarez MA, Wise JH, Abel T. ApJ. 2009; 701:L133.
- Appenzeller I, Fricke K. A&A. 1972; 21:285.
- Bañados E, et al. Nature. 2018; 553:473. [PubMed: 29211709]
- Baumgarte TW, Shapiro SL. ApJ. 1999a; 526:937.
- Baumgarte TW, Shapiro SL. ApJ. 1999b; 526:941.
- Begelman MC. MNRAS. 2010; 402:673.
- Begelman MC, Rees MJ. MNRAS. 1978; 185:847.
- Begelman MC, Volonteri M, Rees MJ. MNRAS. 2006; 370:289.
- Bisnovatyi-Kogan GS. ApJ. 1998; 497:559.
- Bisnovatyi-Kogan GS, Zel'dovich YB, Novikov ID. Soviet Ast. 1967; 11:419.
- Bond JR, Arnett WD, Carr BJ. ApJ. 1984; 280:825.
- Bowler RAA, McLure RJ, Dunlop JS, McLeod DJ, Stanway ER, Eldridge JJ, Jarvis MJ. MNRAS. 2017; 469:448.
- Bromm V, Loeb A. ApJ. 2003; 596:34.
- Chandrasekhar S. An Introduction to the Study of Stellar Structure University of Chicago Press; Chicago, IL: 1939

- Chandrasekhar S. *Phys Rev Lett*. 1964; 12:114.
- Clayton DD. *Principles of Stellar Evolution and Nucleosynthesis* University of Chicago Press; Chicago, IL: 1983
- Eddington AS. *ApJ*. 1918a; 48:205.
- Eddington AS. *MNRAS*. 1918b; 79:2.
- Fan X. *New Astron Rev*. 2006; 50:665.
- Fan X, et al. *AJ*. 2006; 131:1203.
- Fryer CL, Woosley SE, Heger A. *ApJ*. 2001; 550:372.
- Fuller GM, Woosley SE, Weaver TA. *ApJ*. 1986; 307:675.
- Haemmerlé L, Woods TE, Klessen RS, Heger A, Whalen DJ. *MNRAS*. 2018a; 474:2757.
- Haemmerlé L, Woods TE, Klessen RS, Heger A, Whalen DJ. *ApJ*. 2018b; 853:L3.
- Haiman Z. *ApJ*. 2004; 613:36.
- Haiman Z. *Astrophysics and Space Science Library*. In: Wiklind T, Mobasher B, , Bromm V, editors *The First Galaxies* Vol. 396. Springer; Berlin: 2013 293
- Hartwig T, et al. *MNRAS*. 2016; 462:2184.
- Heger A, Woosley SE. *ApJ*. 2002; 567:532.
- Heger A, Fryer CL, Woosley SE, Langer N, Hartmann DH. *ApJ*. 2003; 591:288.
- Hosokawa T, Yorke HW, Inayoshi K, Omukai K, Yoshida N. *ApJ*. 2013; 778:178.
- Hoyle F, Fowler WA. *MNRAS*. 1963; 125:169.
- Iben I Jr. *ApJ*. 1963; 138:1090.
- Johnson JL, Whalen DJ, Li H, Holz DE. *ApJ*. 2013; 771:116.
- Kippenhahn R, , Weigert A, , Weiss A. *Stellar Structure and Evolution 2*. Springer; Berlin: 2012
- Koushiappas SM, Bullock JS, Dekel A. *MNRAS*. 2004; 354:292.
- Lai D, Rasio FA, Shapiro SL. *ApJS*. 1993; 88:205.
- Latif MA, Ferrara A. *PASA*. 2016; 33:e051.
- Latif MA, Schleicher DRG, Schmidt W, Niemeyer J. *MNRAS*. 2013; 433:1607.
- Li Y, Klessen RS, Mac Low M-M. *ApJ*. 2003; 592:975.
- Liu YT, Shapiro SL, Stephens BC. *Phys Rev D*. 2007; 76:084017.
- Lodato G, Natarajan P. *MNRAS*. 2006; 371:1813.
- Loeb A, Rasio FA. *ApJ*. 1994; 432:52.
- Lupi A, Haardt F, Dotti M, Fiacconi D, Mayer L, Madau P. *MNRAS*. 2016; 456:2993.
- Madau P, Rees MJ. *ApJ*. 2001; 551:L27.
- Maeder A, Meynet G. *A&A*. 2000; 361:159.
- Mayer L, Fiacconi D, Bonoli S, Quinn T, Roškar R, Shen S, Wadsley J. *ApJ*. 2015; 810:51.
- McLaughlin GC, Fuller GM. *ApJ*. 1996; 456:71.
- Milosavljević M, Bromm V, Couch SM, Oh SP. *ApJ*. 2009; 698:766.
- Montero PJ, Janka H-T, Müller E. *ApJ*. 2012; 749:37.
- Mortlock DJ, et al. *Nature*. 2011; 474:616. [PubMed: 21720366]
- Oh SP, Haiman Z. *ApJ*. 2002; 569:558.
- Oppenheimer JR, Volkoff GM. *Phys Rev*. 1939; 55:374.
- Ostriker JP, Hartwick FDA. *ApJ*. 1968; 153:797.
- Pacucci F, Volonteri M, Ferrara A. *MNRAS*. 2015; 452:1922.
- Planck Collaboration XIII. *A&A*. 2016; 594:A13.
- Rees MJ. *ARA&A*. 1984; 22:471.
- Regan JA, Haehnelt MG. *MNRAS*. 2009a; 393:858.
- Regan JA, Haehnelt MG. *MNRAS*. 2009b; 396:343.
- Sakurai Y, Hosokawa T, Yoshida N, Yorke HW. *MNRAS*. 2015; 452:755.
- Sakurai Y, Inayoshi K, Haiman Z. *MNRAS*. 2016; 461:4496.
- Schleicher DRG, Palla F, Ferrara A, Galli D, Latif M. *A&A*. 2013; 558:A59.

- Shapiro SL. *Coevolution of Black Holes and Galaxies* Ho LC, editor Cambridge Univ. Press; Cambridge: 2004 103
- Shapiro SL. *ApJ*. 2005; 620:59.
- Shapiro SL. *Phys Rev D*. 2017; 95:101303. [PubMed: 29881790]
- Shapiro SL, Shibata M. *ApJ*. 2002; 577:904.
- Shapiro SL, Teukolsky SA. *Black Holes, White Dwarfs, and Neutron Stars: The Physics of Compact Objects* Wiley Interscience; New York: 1983
- Shibata M, Shapiro SL. *ApJ*. 2002; 572:L39.
- Shibata M, Sekiguchi Y, Uchida H, Umeda H. *Phys Rev D*. 2016a; 94:021501.
- Shibata M, Uchida H, Sekiguchi Y-i. *ApJ*. 2016b; 818:157.
- Smith A, Bromm V, Loeb A. *MNRAS*. 2016; 460:3143.
- Smith A, Bromm V, Loeb A. *Astron Geophys*. 2017; 58:3.22.
- Sobral D, Matthee J, Darvish B, Schaerer D, Mobasher B, Röttgering HJA, Santos S, Hemmati S. *ApJ*. 2015; 808:139.
- Spitzer LJ. *Physical Processes in the Interstellar Medium* Wiley-Interscience; New York: 1978
- Sun L, Paschalidis V, Ruiz M, Shapiro SL. *Phys Rev D*. 2017; 96:043006.
- Tanaka TL. *Class Quantum Grav*. 2014; 31:244005.
- Tanaka T, Haiman Z. *ApJ*. 2009; 696:1798.
- Tolman RC. *Phys Rev*. 1939; 55:364.
- Uchida H, Shibata M, Yoshida T, Sekiguchi Y, Umeda H. *Phys Rev D*. 2017; 96:083016.
- Umeda H, Hosokawa T, Omukai K, Yoshida N. *ApJ*. 2016; 830:L34.
- Visbal E, Haiman Z, Bryan GL. *MNRAS*. 2014; 442:L100.
- Volonteri M, Rees MJ. *ApJ*. 2005; 633:624.
- Volonteri M, Haardt F, Madau P. *ApJ*. 2003a; 582:559.
- Volonteri M, Madau P, Haardt F. *ApJ*. 2003b; 593:661.
- Volonteri M, Silk J, Dubus G. *ApJ*. 2015; 804:148.
- Wagoner RV. *ARA&A*. 1969; 7:553.
- Whalen DJ, Fryer CL. *ApJ*. 2012; 756:L19.
- Wise JH, Turk MJ, Abel T. *ApJ*. 2008; 682:745.
- Woods TE, Heger A, Whalen DJ, Haemmerlé L, Klessen RS. *ApJ*. 2017; 842:L6.
- Wu XB, et al. *Nature*. 2015; 518:512. [PubMed: 25719667]
- Yoon S-C, Kang J, Kozyreva A. *ApJ*. 2015; 802:16.
- Zeldovich YB, Novikov ID. *Relativistic Astrophysics. Vol.1: Stars and Relativity* University of Chicago Press; Chicago, IL: 1971

APPENDIX A: THE DARK MATTER CONTRIBUTION TO THE STELLAR ENERGY

In this appendix, we derive approximations for the contribution of a DM halo on the energy of an SMS, considering the opposite extremes of CDM and HDM. We imagine that the SMS is surrounded by a much larger region filled with DM particles that are collision-less, monoenergetic and moving isotropically. Far from the SMS, the DM has a uniform density $\rho_{\text{DM}}^{\infty}$ and the particle speed is $v_{\infty} \ll 1$. A simple phase-space distribution function describing this DM is

$$f = f(E) = \rho_{\text{DM}}^{\infty} \frac{\delta(E - E_{\infty})}{4\pi(2E_{\infty})^{1/2}}, \quad (\text{A1})$$

where the asymptotic energy per unit mass is $E_{\infty} = v_{\infty}^2/2$ [see equation (ST.14.2.16)].

Integrating over the distribution function, we find for the density

$$\rho_{\text{DM}} = \rho_{\text{DM}}^{\infty} \left(1 - \frac{2\Phi_{\text{SMS}}}{v_{\infty}^2}\right)^{1/2} \quad (\text{A2})$$

[compare equation (ST.14.2.22)].

Strictly speaking, the above distribution function holds only for stationary configurations. It is also a very good approximation for the quasi-stationary situation encountered when we consider small oscillations of the equilibrium configuration. Justification of this approximation is provided by the following argument (McLaughlin & Fuller 1996) which suggests that the DM density is at most very weakly affected by the oscillations of the SMS.

Consider a DM particle with zero speed v_{∞} at a large separation from the SMS. Once it has reached the surface of the SMS, it will travel at the escape speed $v \simeq (GM/R)^{1/2}$, and will therefore transverse the star in a time of approximately $\tau_{\text{cross}} \sim R/v \sim (R^3/\lambda GM)^{1/2} \sim (G\rho)^{-1/2} \sim \tau_{\text{ff}}$, where τ_{ff} is the free-fall time. The crossing time τ_{cross} will be even shorter for particles with $v_{\infty} > 0$ at large separation, so that $\tau_{\text{cross}} \lesssim \tau_{\text{ff}}$ in general. For stars with structures similar to $n = 3$ polytropes, the fundamental radial oscillation period τ_{osc} is larger than the free-fall time, which establishes the inequality $\tau_{\text{cross}} < \tau_{\text{osc}}$. In fact, for stars near the critical configuration, the oscillation frequency approaches zero, so that τ_{osc} becomes infinite. Assuming spherical symmetry, DM particles are unaffected by oscillations of the SMS, while they are outside of the star, because the exterior potential will not change. Since Φ_{SMS} varies on the time-scale τ_{osc} , which is longer than the crossing time τ_{cross} , the quasi-stationary approximation applies, and hence we may adopt equation (A2).

We now consider two opposite extreme limits, namely $2\Phi_{\text{SMS}}/v_{\infty}^2 \gg 1$ and $2\Phi_{\text{SMS}}/v_{\infty}^2 \ll 1$, where Φ_{SMS} is evaluated inside the SMS. The former applies in the limit when the speed of the DM particles is much less than the escape speed from the SMS, which we refer to as CDM. Conversely, the latter applies when the DM particles are much faster than the escape speed, which we refer to as HDM. We treat these two limits separately in the following two sections. At large distances from the SMS, we always have $\Phi_{\text{SMS}} \rightarrow 0$, so that, from equation (A2), we always have $\rho_{\text{DM}} \rightarrow \rho_{\text{DM}}^{\infty}$ in both limits, as expected.

A1 Cold dark matter

In a region where $2\Phi_{\text{SMS}}/v_{\infty}^2 \gg 1$, we may approximate equation (A2) as

$$\rho_{\text{CDM}} \simeq \rho_{\text{DM}}^{\infty} \left(-\frac{2\Phi_{\text{SMS}}}{v_{\infty}^2} \right)^{1/2}. \quad (\text{A3})$$

We now invoke a further approximation and argue that, given the large central condensation of an $n = 3$ polytrope, we may crudely approximate the potential of the SMS as that of a point mass, so that

$$\rho_{\text{CDM}} \simeq \rho_{\text{DM}}^{\infty} \left(\frac{2M}{rv_{\infty}^2} \right)^{1/2}. \quad (\text{A4})$$

The Newtonian potential caused by the DM distribution can then be found from the Poisson equation

$$\nabla^2 \Phi_{\text{CDM}} = \frac{1}{r^2} \frac{d}{dr} \left(r^2 \frac{d\Phi_{\text{CDM}}}{dr} \right) = 4\pi\rho_{\text{CDM}}. \quad (\text{A5})$$

Inserting equation (A4) and integrating twice, we obtain

$$\Phi_{\text{CDM}} = 2^{1/2} \frac{16\pi \rho_{\text{DM}}^{\infty} M^{1/2}}{15 v_{\infty}} r^{3/2} + C, \quad (\text{A6})$$

where C is a constant of integration, and where we have set a second constant of integration to zero in order to make Φ_{CDM} regular at the origin. We can now find the contribution of this potential to the energy of the SMS from

$$\begin{aligned} E_{\text{CDM}} &= \int_0^M \Phi_{\text{CDM}} dm = 4\pi \int_0^R \Phi_{\text{CDM}} \rho r^2 dr \quad (\text{A7}) \\ &= 2^{1/2} \frac{64\pi^2 \rho_{\text{DM}}^{\infty} M^{1/2}}{15 v_{\infty}} \int_0^R \rho r^{7/2} dr. \end{aligned}$$

Here, the integration is carried out over the SMS, we have assumed spherical symmetry, and we have omitted the constant C in equation (A6), since it would lead to a term that is

independent the density, and which would therefore drop out when we take derivatives of the energy with respect to the density. To leading order, the structure of the SMS is that of an $n = 3$ polytrope, so that we can rewrite the last integral in equation (A7) using Lane–Emden variables $\rho = \rho_c \theta^3$ and $r = a_{\text{LE}} \xi$ with $a_{\text{LE}} = K^{1/2} \rho_c^{-1/3} / \pi^{1/2}$

$$\begin{aligned} E_{\text{CDM}} &= 2^{1/2} \frac{64}{15\pi^{1/4}} \frac{\rho_{\text{DM}}^\infty M^{1/2}}{v_\infty} \rho_c a_{\text{LE}}^{9/2} \int_0^{\xi_3} \theta^3 \xi^{7/2} d\xi \quad (\text{A8}) \\ &= 2^{1/2} \frac{64}{15\pi^{1/4}} \frac{\rho_{\text{DM}}^\infty M^{1/2}}{v_\infty} \rho_c^{-1/2} K^{9/4} \int_0^{\xi_3} \theta^3 \xi^{7/2} d\xi. \end{aligned}$$

We now define

$$k_{\text{CDM}} \equiv 2^{1/2} \frac{64}{15\pi^{1/4}} \int_0^{\xi_3} \theta^3 \xi^{7/2} d\xi = 30.0193 \quad (\text{A9})$$

and use the dimensional rescaling $\bar{E} = K^{-3/2} E$ (and similar for M) together with equation (34) and

$$x_{\text{DM}} = M^{2/3} (\rho_{\text{DM}}^\infty)^{1/3} \quad (\text{A10})$$

to obtain the rescaled energy

$$\bar{E}_{\text{CDM}} = k_{\text{CDM}} x_{\text{DM}}^3 v_\infty^{-1} \bar{M}^{-1/2} x^{-3/2}. \quad (\text{A11})$$

We may now account for the effects of CDM by including this term in the energy equation (65).

A2 Hot dark matter

In the opposite limit, $2\Phi_{\text{SMS}}/v_\infty^2 \ll 1$, the DM density is unaffected by the SMS and takes the constant value

$$\rho_{\text{HDM}} \simeq \rho_{\text{DM}}^\infty, \quad (\text{A12})$$

which is the regime considered by McLaughlin & Fuller (1996) and Bisnovatyi-Kogan (1998). Solving the Poisson equation (A5) for the potential Φ_{HDM} , we obtain

$$\Phi_{\text{HDM}} = \frac{2\pi}{3}\rho_{\text{DM}}^{\infty}r^2, \quad (\text{A13})$$

where we have omitted two constants of integration for the same reasons as in Appendix A1. The contribution of this potential to the energy of the SMS is then

$$\begin{aligned} E_{\text{HDM}} &= \int_0^M \Phi_{\text{HDM}} dm = 4\pi \int_0^R \Phi_{\text{HDM}} \rho r^2 dr \quad (\text{A14}) \\ &= \frac{8\pi^2}{3}\rho_{\text{DM}}^{\infty} \int_0^R \rho r^4 dr. \end{aligned}$$

As in Appendix A1, we use Lane–Emden variables for an $n = 3$ polytrope to rewrite this integral as

$$\begin{aligned} E_{\text{HDM}} &= \frac{8\pi^2}{3}\rho_{\text{DM}}^{\infty}\rho_c a_{\text{LE}}^5 \int_0^{\xi_3} \theta^3 \xi^4 d\xi \quad (\text{A15}) \\ &= \frac{8}{3\pi^{1/2}}K^{5/2}\rho_{\text{DM}}^{\infty}\rho_c^{-2/3} \int_0^{\xi_3} \theta^3 \xi^4 d\xi. \end{aligned}$$

We now define

$$k_{\text{HDM}} = \frac{8}{3\pi^{1/2}} \int_0^{\xi_3} \theta^3 \xi^4 d\xi = 16.3262. \quad (\text{A16})$$

and adopt the same rescaling as in Appendix A1 to find the rescaled energy

$$\bar{E}_{\text{HDM}} = k_{\text{HDM}} \bar{M}^{-2/3} x_{\text{DM}}^3 x^{-2}. \quad (\text{A17})$$

In order to account for a hot dark-energy halo, we therefore add this term to the energy equation (65).

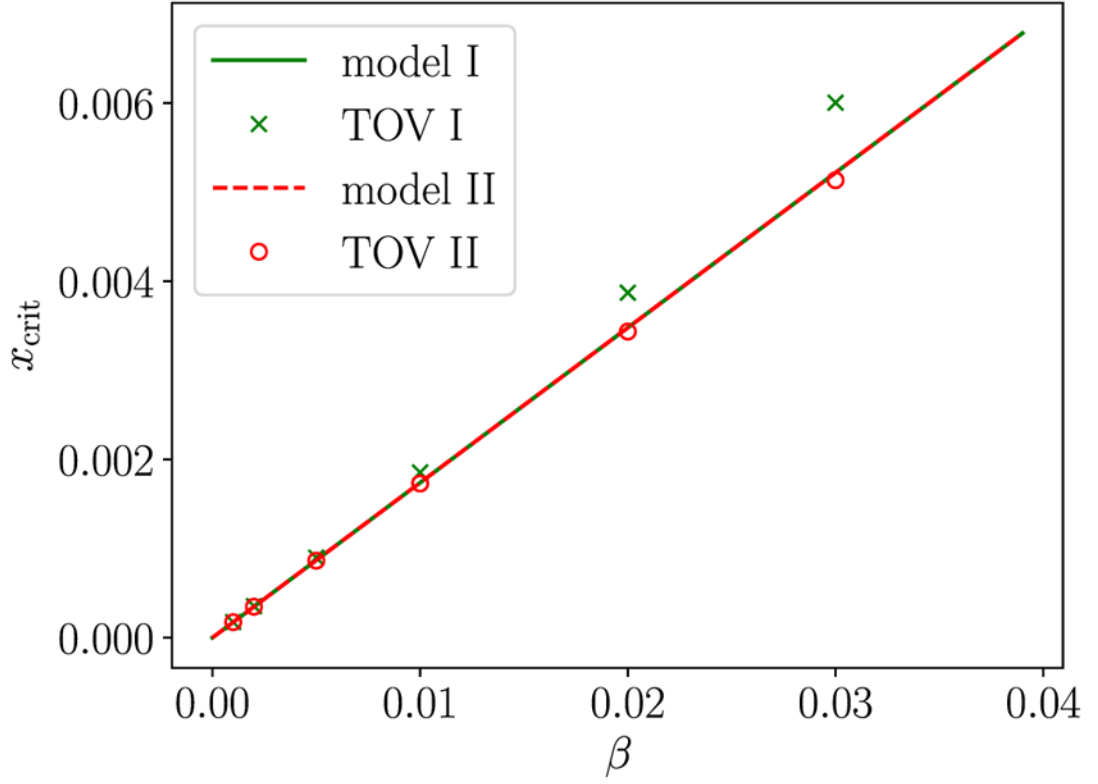


Figure 1.

The density variable $x_{\text{crit}} = M_{\text{crit}}^{2/3} \rho_{\text{crit}}^{1/3}$ as a function of β for non-rotating SMSs according to Approaches I and II. Crosses and circles denote the numerical results from Section 3.1, using Approaches I and II, while the lines represent the analytical, perturbative predictions (49) and (56) from Section 3.2 (which are identical for Approaches I and II).

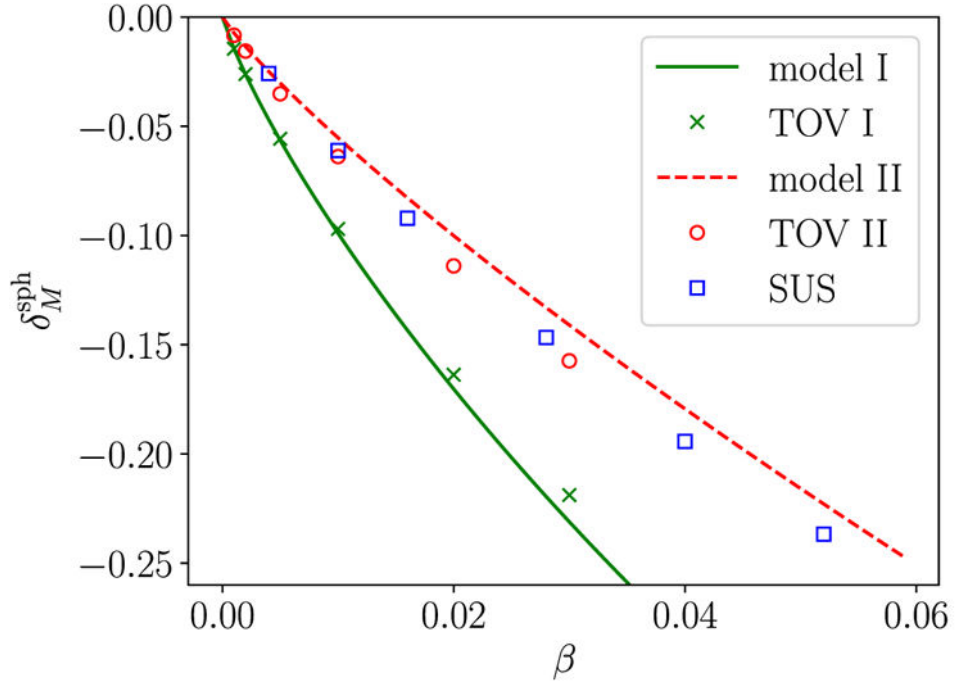


Figure 2.

The relative change in the mass δ_M^{sph} [see equation (36)] as a function of β for non-rotating SMSs according to Approaches I and II. Crosses and circles denote the numerical results from Section 3.1, while the solid and dashed lines represent the analytical, leading-order predictions (51) and (60) from Section 3.2. Note the non-linear behaviour of the analytical predictions, which are caused by the logarithmic terms in equations (51) and (60). The squares labelled SUS represent numerical results of SUS, who adopted Approach II.

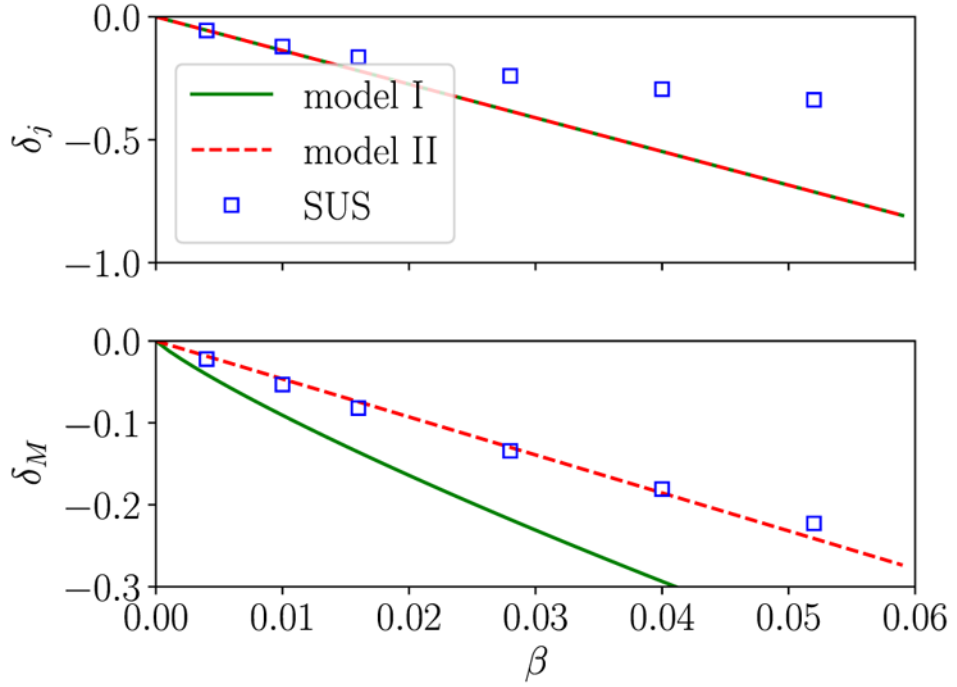


Figure 3. Effects of gas pressure on the dimensionless angular momentum j and the rescaled mass \bar{M} of the critical configuration of rotating SMSs. We show δ_j and δ_M , defined in equations (83) and (84), as a function of β . The solid and dashed lines represent our analytical perturbative expressions according to models I and II, while the squares represent the numerical results of SUS.

Table 1

Values of the structure coefficients k_i for $n = 3$ polytropes.

Coefficient	Value	Reference
k_1	1.7558	Lai et al. (1993)
k_2	0.63899	Lai et al. (1993)
k_3	1.2041	Lai et al. (1993)
k_4	0.918294	ST
k_5	0.331211	Lombardi (private communication)
k_τ	-0.45928	equation (44)
k_{CDM}	30.0193	equation (A9)
k_{HDM}	16.3262	equation (A16); Bisnovatyi-Kogan (1998)

Table 2

Characteristic parameters of the unperturbed critical configuration.

Calculation	$(R_p/M)_{\text{crit}}$	x_0	J_{min}	J_0	M_0
Paper I; analytical	456	5.15×10^{-3}	0.8733	0.8757	4.5551
Paper I; numerical	427	5.26×10^{-3}	0.882	0.97	4.57
SUS				0.921	4.56

Table 3Comparison of estimates for δ_j , δ_x , and δ_M^{II} .

Calculation	δ_j/β	δ_x/β	$\delta_M^{\text{II}}/\beta$
Paper I; analytical	-16.7	33.4	-4.7
Paper I; numerical	-11.4	22.8	-4.6
SUS	-13.7	27.4	-4.6